Silicon (2024) 16:4577–4607
https://doi.org/10.1007/s12633-024-03034-4

REVIEW

Exploring Eco-Friendly Green Synthesis of Calcium Silicate and its Derivatives for Diverse Applications

Pooja Yadav[1] · Sushil Patel[1] · Gangadhar Mahar[1] · Krishnam Raju[1] · P. Abdul Azeem[1]

Received: 18 February 2024 / Accepted: 23 May 2024 / Published online: 11 June 2024

Abstract

Calcium oxide and silicon oxide are combined to form calcium silicate. Since calcium silicate materials offer tuneable physical, chemical, mechanical, and optical characteristics, these materials have found uses in various applications such as luminescence, batteries, bioimaging, supercapacitors, and concrete materials. In the majority of applications, high-purity calcium silicate is produced from chemical precursors such as calcium/silicate oxides or nitrites, even though this method could be expensive, environmentally harmful, and non-biocompatible. As an alternative, natural calcium and silica from biomass are usually economical and abundant, yet they contain impurities but sometimes the trace impurities influence the properties of material in positive ways. Silica can be extracted from wheat husk, rice husk, and sugarcane bagasse, which are frequently dumped in rivers, ponds, and other water bodies, contributing to ecological and health problems, likewise, calcium oxide can be extracted from eggshells, marble waste, snail shell. The trash may recycle or utilized to create marketable, value-added items with significant ecological and financial benefits rather than being dumped. The purpose of this review paper is to discuss the composition, processing, and applications of calcium silicate derivatives. The analysis shows that calcium silicate derivatives have enormous potential for using waste as a replacement of organic precursor materials.

Keywords Recycling waste · Environmentally friendly · Calcium silicate · Green synthesis · Food waste · Industrial waste · Agricultural waste

Abbreviations

CS	Calcium Silicate
FA	Fly Ash
GGBS	Ground Granulated Blast furnace slag
GDP	Gross domestic product
USDA	United States Department of Agriculture
SiO2	Silica
ES	Eggshells
CaCO3	Calcium carbonate
UCC	Unburnt carbon content
HCl	Hydrochloric acid
HF	Hydrogen fluoride acid
HNO3	Nitric acid
H2SO4	Sulfuric acid
SCBA	Self-compacting concrete
CTAB	Cetyltrimethylammonium bromide
NCS	Natural calcium silicate
CCS	Chemical calcium silicate
OPL	Oil palm leaves
TEOS	Tetraethyl orthosilicate
SBF	Simulated body fluid
CPC	Calcium phosphate cement
HA	Hydroxyapatite
BTE	Bone tissue engineering
FDA	Food and Drug Administration
CSH	Calcium silicate hydrate
MCS	Mesoporous calcium silicate
LEDs	Light-emitting diodes
PGMS	Propylene glycol modified silane
PL	Photoluminescence

✉ P. Abdul Azeem
drazeem2002@nitw.ac.in

[1] Department of Physics, National Institute of Technology, Warangal 506004, India

1 Introduction

Calcium silicates (CS) and their derivatives have been extensively used in various applications such as luminescence, optical sensors [1], solar cell, bioimaging agents [2], drug delivery, and tissue engineering [3]. CS materials offer excellent biocompatibility, biodegradability, and exhibit

bioactive behavior means when implanted in the body, the material forms a layer of hydroxyapatite [4]. CS in bone tissue engineering offers a promising approach to promote bone regeneration, repair bone defects, and enhance the integration of implants with natural bone. CS nanoparticles can be used as drug delivery vehicles for targeted drug delivery because it is a low-density material [5]. Functionalization of these nanoparticles with targeting moieties, such as antibodies or peptides, allows for precise targeting of cancer cells or diseased tissues. Once the nanoparticles reach the target site, the drug can be released to provide localized treatment [6]. Also it holds a great potential for addressing environmental challenges and harnessing renewable energy sources through the utilization of light energy for various chemical processes. These materials exhibit photo catalytic activity, excellent stability, durability, and possess a wide band gap that allows them to absorb light in the ultraviolet (UV) region of the electromagnetic spectrum [7]. The combination of its photo catalytic properties, stability, wide band gap, low toxicity, and versatility makes CS a useful material in photo catalyst applications. Moreover, CS and its derivatives are also used in sensing applications such as gas sensors. Due to the high surface area of the material it provides a large active surface for gas interactions [8]. According to reports, the utilization of CS nanosheets has been introduced to create gas sensors with exceptional stability in different humidity conditions [9]. Due to the hygroscopic properties of CS nanosheets, they possess the ability to selectively trap water molecules within their structure. This unique characteristic allows for the adsorption of target gas molecules onto the active material surface without any interference from the water molecules. Moreover, the two-dimensional arrangement of CS nanosheets offers a remarkable surface-to-volume ratio, thereby maximizing the capacity for adsorbing water molecules onto their surfaces [10]. Furthermore, they are utilized as host materials in luminescence applications due to their low phonon energy, good chemical stability, high transparency to visible light, and ability to accommodate different activator ions [11]. CS exhibits high luminescence efficiency when it is doped with some rare-earth ions. They can exhibit strong and tunable emission in a wide range of colors, depending on the choice of activated ion. The emission can span from the visible to the near-infrared region of the electromagnetic spectrum. Additionally, CS has good thermal stability and can withstand high temperatures, making it suitable for applications where heat resistance is required. It occupies a prime position in display and forensic applications due to its facile synthesis and optimized properties like chemical stability, thermal stability, mechanical stability, and optoelectronic [12, 13].Each day, we come across a diverse array of agricultural, food, and industrial products that serve our needs and make our lives easier. Agricultural activities contribute significantly to the Gross Domestic Product (GDP) of many countries. This includes not only the direct output of crops and livestock but also the various supporting industries such as equipment manufacturing, food processing, transportation, and distribution. Furthermore, industries such as steel, mineral processing, paper, and pulp also play a vital role in shaping human existence and well-being [14]. These two categories of industries are responsible for meeting our everyday needs. The development and advancement of industries are key indicators of a country's progress. However, a significant drawback associated with these industries is the production of millions of tonnes of by-products on a daily basis worldwide [15]. So, utilizing waste material is a major problem all across the world. The increasing global population is driving the demand for industrialization to meet the needs of people. However, this industrialization comes at a cost to the ecosystem, resulting in the generation of excessive waste and environmental pollution [16]. Traditionally, there is increasing interest in using bio-waste-derived ceramic, phosphor material [17, 18]. Opting for biowaste is a sustainable and cost-effective process as it utilizes waste materials that would otherwise be disposed of in landfills or incinerated and it is a cost-effective process as the raw materials are readily available and inexpensive [19]. The primary focus of researchers lies in biowaste-derived CS, as they have observed more pronounced improvements in both the material's structural and optical characteristics compared to those derived through chemical processes [20]. Bio-waste materials also enhanced the chemical stability of the prepared material due to the presence of organic components in the biowaste, which can form stable complexes with heavy metals and prevent their leaching. The biomass CS can be produced by the combination of calcium source and silica source extracted from the waste material. As silicon oxide and calcium oxide are the major elements found in the earth’s crust. Indeed, waste materials such as eggshells and seashells are rich sources of calcium carbonate, a compound found abundantly in nature [21]. Likewise, rice husk, coconut husk, sugarcane bagasse, peanut shell, bamboo leaves, and many more waste materials are abundant sources of silicon oxide [22] as shown in Fig. 1, and are utilized in the extraction of useful components for various applications and purposes. Industrial wastes such as fly ash (FA) and ground granulated blast furnace slag (GGBS) are the excess waste generated from the iron and steel industry respectively. In thermal power plants, the by-product obtained after the coal burning is named FA [23]. In India, 196 million tonnes of FA are generated every year [24]. Typically, such waste is often indiscriminately dumped in open areas or water resources. As temperatures rise, the lightweight waste becomes airborne and can enter the human body through the respiratory system, impacting not only humans but also animals, birds, and aquatic species [25]. From 1937 onwards, FA is used in the cement

Fig. 1 Different types of waste are generated from food, agricultural, and industrial sources

industries usually in concrete and brick production because of its significant properties like porosity, lightweight, high surface area, and low bulk density [26].

Mostly FA is used as a catalyst in various applications to reduce the cost of raw materials and production costs. The second industrial waste is GGBS, which is obtained from the iron and steel industry. During the production of iron and steel making, quenching molten slag comes out from the blast furnace which is further dried and ground into a fine powder named as GGBS [27]. The obtained slag is a rich source of calcium silicate hydrates, which is used in cement production or concrete production to enhance the strength and durability of the cement [28]. Apart from industrial waste and food waste, agricultural waste also creates environmental problems. The food and agricultural waste are bio-degradable waste, but the degradation process is lengthy and it requires a lot of land area [29]. The most abundant amount of waste generated is rice husk. Rice husk is a major amount of waste generated from the rice crop. According to the United States Department of Agriculture (USDA), the global rice production for the 2019/2020 period was projected to be approximately 499.31 million metric tons. In the previous year, 2018/2019, the production stood at 499.37 million metric tons (World agricultural production, 2020). It is estimated that during the milling process of rice, each kilogram of rice would yield approximately 0.28 kg of rice husk [30]. Consequently, a substantial quantity of rice husk is generated. However, due to the lack of effective utilization methods, this husk is often burned or left to become airborne, resulting in environmental pollution. Farmers typically aim to clear their fields quickly after the harvest to prepare for the next crop. Unfortunately, the natural degradation process of agricultural waste is time-consuming. As a result, and due to limited waste management options and high costs, burning the crop residue remains the only viable choice for many farmers. This practice contributes to air pollution and has adverse effects on the climate [31]. Rice husk chemical composition contains a major amount of silica (SiO_2) as shown in Table 1 and a global pie chart of the different waste produced annually in different countries is shown in Fig. 2.

In the food industry, major waste is generated from eggs. Eggshells (ES) are the hard outer covering of the eggs and it is composed mainly of calcium carbonate, which gives protection to the embryo inside the egg [32]. Decomposing of ES creates various issues such as taking a long time to decompose in landfills due to calcium carbonate composition, and it takes several years for proper decomposition [21]. Furthermore, improper disposal of ES, such as being

Table 1 Chemical composition of the waste generated from the food, agricultural and industrial sources

Chemical Composition (%)								
Oxide Compounds	Rice husk	Eggshell	Sugarcane Bagasse	Snail Shell	Coconut Husk	Peanut Shell	Fly Ash	GGBS
Calcium oxide (CaO)	0.49	92.823	2.8	97.14	4.98	11.23	2.9	45.8
Silicon dioxide (SiO_2)	93.0	0.363	73	0.628	37.97	41.42	63.1	30.1
Strontium oxide (SrO)	-	0.246	-	0.457	-	-	-	-
Iron oxide (Fe_2O_3)	0.13	-	6.3	0.409	15.48	12.60	6.5	5.7
Sodium oxide (Na_2O)	0.02	-	1.1	0.336	0.95	1.02	-	0.2
Manganese oxide (MnO)	-	-	-	0.308	0.81	0.23	-	-
Potassium oxide (K_2O)	1.03	0.311	2.4	0.212	0.83	11.89	1.1	1.2
Aluminium oxide (Al_2O_3)	0.20	0.238	6.7	0.180	24.12	11.75	23.3	13.4
Magnesium oxide (MgO)	0.73	1.179	3.2	0.152	1.89	3.51	1.2	6.1
Chromium oxide (Cr_2O_3)	-	-	-	0.083	-	-	-	-

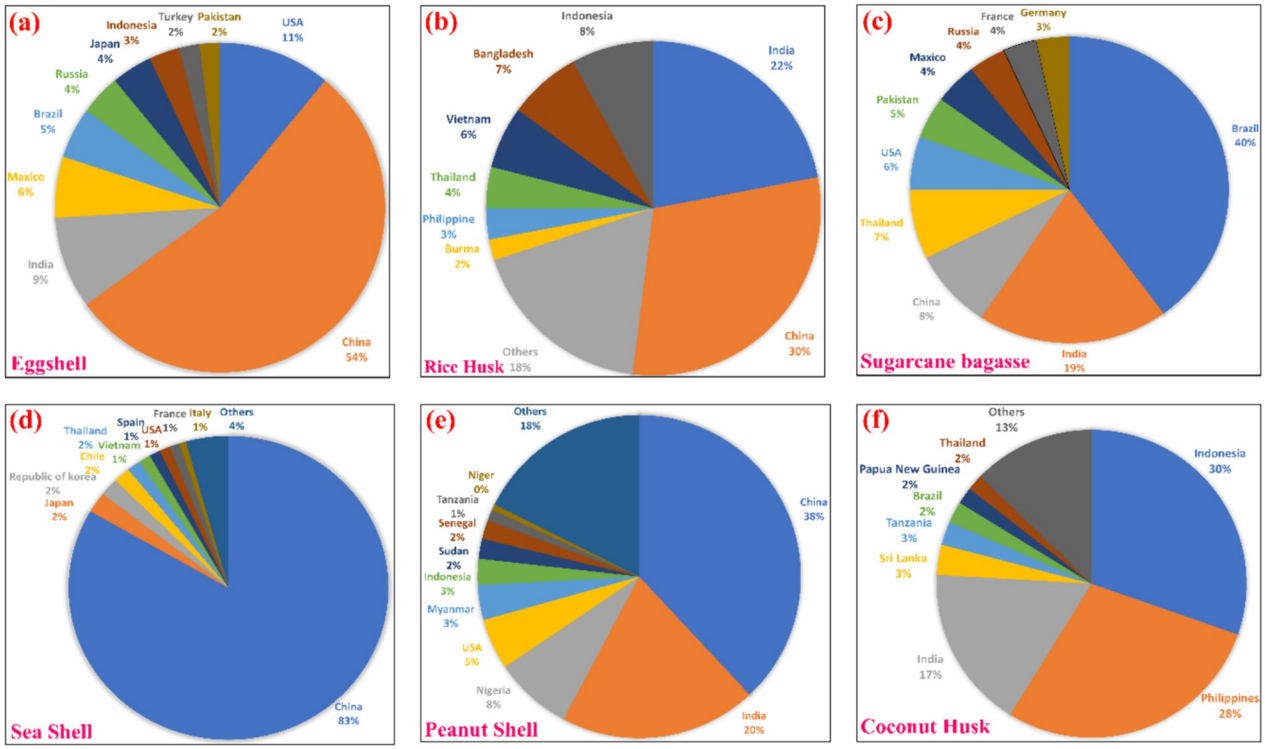

Fig. 2 Global pie chart of (**a**) eggshell (**b**) rice husk (**c**) sugarcane bagasse (**d**) sea shell (**e**) peanut shell (**f**) coconut husk produced annually in different countries

discarded in standard household waste, can contribute to the emission of greenhouse gases like methane, carbon dioxide, and nitrous oxide [33]. So, various issues like landfill, availability, odour insects, abrasiveness, climate change, and global warming make ES as a waste product. Globally egg production up to 2017 is 80 million metric tons per year [34]. In egg production, India is the third-largest producer in the world. Over the last many years, ES are utilized to generate various valuable products by incorporating them with commercial products due to their impressive chemical and physical properties like high thermal stability, mechanical properties, flame resistance, and many more. It contains a high amount of calcium carbonate ($CaCO_3$) and it is easily available in bulk amounts, lightweight, and eco-friendly.

Another major waste originating from the agricultural industry is sugarcane bagasse. After the extraction of juices from the sugarcane for sugar manufacture, the left behind the product is sugarcane bagasse. Bagasse is a renewable resource that can be used as a biofuel and as a raw material in the making of paper, board, and other products [35]. There are various ways to properly dispose of bagasse, such as using it for composting, as a soil amendment, or as animal feed. It is available in abundant and can provide a sustainable source of energy and materials, but can create waste and pollute the environment if not managed properly [36]. But some farmers burnt the bagasse, which will create environmental pollution because the low-temperature burning can release harmful pollutants such as sulphur dioxide, nitrogen oxides, and particulate matter [37]. Sugarcane is grown in a major area across many countries like Brazil, India, Australia, and South Africa. Yearly, India only produces 40 million metric tonnes of bagasse and it contains a major amount of silica oxide in it with other trace elements [38]. One more waste is coconut husk, which is an outer covering of coconut fruit. It is a tough, fibrous material that surrounds the inner flesh of the coconut. The fibrous layer of coconut is the mesocarp and the smooth layer is known as the exocarp. When the coconut husk is heated at a higher temperature it can convert into silica. India is the largest coconut-producing country in the world [39]. According to the 2020 survey by the food and agriculture organization of the United Nations, India produced around 21.3 billion coconuts, which is more than 20% of the world's total coconut production. Indonesia, Philippines, Vietnam, Sri Lanka, Thailand, and Mexico also produce a major amount of coconut. A peanut shell is the outer covering of the peanut. The shell of a peanut is not typically eaten, as it is difficult to digest and does not have any nutritional value. Some people can be allergic to peanuts and even handling the shell can trigger an allergic reaction in some individuals [40]. However, there are a variety of uses for shells, such as animal feed or a fuel source. They can be used as a soil amendment in gardening as they

help to improve soil structure and retain moisture. India is the top five producers of peanuts in the world. According to the United States Department of Agriculture, India produced approximately 7.9 million metric tons of peanuts in the 2020–2021 season. Globally, an estimated 47 million metric tons are produced annually. Apart from other waste, seashell pollution is a major concern all over the world. Seashell buildup in natural settings has a detrimental effect on the ecosystem, wildlife, and even human health [41]. The causes of seashell pollution are varied, including commercial collection, waste disposal, and unsustainable fishing. The accumulation of seashells on beaches and in oceans can lead to changes in the composition of soil and sand, physical barriers to animal movement, and the absorption of pollutants and chemicals by seashells [42]. To mitigate seashell pollution, it is important to adopt sustainable practices and promote awareness of the ecological importance of seashells. As all the above-mentioned waste contained either a major amount of calcium oxide or silicon oxide. Apart from calcium oxide and silicon oxide, the waste materials also contain a trace number of other impurities such as titanium oxide, magnesium oxide, iron oxide, manganese oxide, aluminum oxide, etc. The chemical composition of the various waste materials obtained from the food industry, agricultural industry, and industrialization as shown in Table 1. These trace elements can be removed by the various synthesis techniques to obtain a pure material, but sometimes their presence also influences the properties of the synthesized material. By combining these silica and calcium sources, calcium silicate and its derivatives (diopside, akermanite) can be synthesized. Comparatively, the usage of biomass in material synthesis and the biomedical industry is less compared to synthetic precursor use because of the less knowledge about the enhancement in the properties by using the biomass. Some of the steps have already been taken by the researchers to find a better use of the above-mentioned toxic waste but proper and effective utilization is still a challenge for researchers.

In this review, our primary focus revolves around the following objectives:

(i) Reducing environmental pollution by converting waste materials into valuable resources.
(ii) Thoroughly investigating multiple extraction methods to obtain calcium oxide and silicon oxide from recycled waste materials, with a focus on optimizing extraction yield.
(iii) Exploring the extraction process of calcium silicate and its derivatives from different sources of calcium oxide and silicon oxide.
(iv) Examining the diverse applications of calcium silicate and its derivatives, encompassing drug delivery, luminescence, and tissue engineering.
(v) Analysing the influence of waste materials on the optical, electrical, and hardness properties of the prepared materials.

2 Calcium and Silica Extraction from Biomass

2.1 Calcium Extraction from Eggshells

Eggshells consist of about 10–11% weight of the total weight of the egg. It is primarily composed of calcium carbonate. Most of the studies concluded that in eggshells 96–97% of calcium carbonate or calcite is present and the rest 3–4% is organic matter such as X collagen, sulfated polysaccharides, and other protein [43]. There are several reports available on pure calcium extraction using eggshells and still research is going on to improve the purity of the final product. Various literature showed that initially, for removing the impurities or dirt, eggshells firstly wash with plain water. After that, for removing the thin organic membrane, the eggshells are put in the boiling waste for some time [34]. Some researchers reported that for removing the organic membrane, it is better to dip eggshells sometimes in a dilute acid solution. In addition, to remove the moisture, keep the shells in a hot air oven for overnight or placed them in sunlight. Heating $CaCO_3$ at high temperatures leads to the formation of calcium oxide and the release of carbon dioxide. Some reports showed that before going for high-temperature calcination, it is good to heat the shells at approx. 450 °C temperature for 2–3 h to remove the organic residues. Thongthai Witoon et al. [44] proposed a method involving the proper cleaning of eggshells followed by calcination at 900 °C under a nitrogen atmosphere. This process resulted in the formation of calcium oxide with a purity of 97.42%. XRD analysis revealed that the intensity of peaks for the commercially available $CaCO_3$ was higher compared to the calcined eggshell. This implies that the CaO crystals in commercially available $CaCO_3$ were larger in size compared to those in the calcined eggshell. A comparative analysis between the calcined eggshell and commercially available $CaCO_3$ was conducted across the relative pressure range of 0.2 to 0.8. The findings indicated that the amount of gas adsorbed by the calcined eggshell was inferior to that of the commercially available $CaCO_3$ after calcination. This suggests that the commercially available $CaCO_3$ possessed a greater number of mesopores and a higher BET surface area. However, this trend reversed at relative pressures surpassing 0.85, implying that the calcined eggshell had a higher proportion of macropores.

Further inquiry unveiled that the calcined eggshell demonstrated a substantial capacity for CO_2 capture due to its carbonation conversion capability. This positions it as a

fitting CO_2 sorbent, attributed to the smaller CaO particle size, which provides an expanded exposed surface area for the surface interaction with CO_2.

Dikshita Nath et al. [45] derived CaO from eggshells and tested it for antibacterial activity. It was observed that the optimum calcination temperature for the formation of calcium oxide is 900 °C. The pictorial representation of the synthesis process is shown in Fig. 3(a). Duncan Cree et al. [46] heated eggshells (ES) and eggshell powder (ESP) at different temperatures (20 °C, 150 °C, 300 °C, 450 °C, 600 °C) to check the heated mortar specimens. At 20 °C, both ES and ESP are white in colour, at 150 °C both turn into pale yellow, at 300 °C they changed into light brown it shows that organic membrane begins to breakdown/decompose, at 450 °C and 600 °C dark gray colour observed. They conclude that little organic membrane is remaining after calcination at 600 °C. Krishna Kumar Jaiswal et al. [47] synthesized calcium oxide with crystallite size ~ 55 nm from chicken eggshells for photocatalytic application. At first, they cleaned eggshells with hot distilled water to remove the fleshy, gelatinous matter and then dried it in a hot air oven at 105 °C for overnight. Then dried eggshell was crushed into a fine powder and calcinated at 900 °C for 3 h with a high heating rate of 15 °C/min and observed that the crystallinity of CaO enhances as the calcination temperature increases. Waseem Ahmad et al. [48] conducted characterization of the outer and inner layers of the raw eggshell, along with powdered eggshell, utilizing FE-SEM, as depicted in Fig. 3(c-d). As illustrated in Fig. 3(c), the surface of the eggshell's exterior presents a smooth texture punctuated by cracks. Figure 3(e) depicts the section of the eggshell that makes up the outer shell, and it demonstrates the protein's fibrous network design, which is very porous in nature. The porous nature of raw eggshells is depicted in Fig. 3(f-g). It was observed that the BET surface area of raw eggshell is $0.56 m^2/g$ and the surface area increase as the calcination temperature increases up to 1000 °C, after that the surface area start decreasing due to the sintering effect. The best adsorption capacity of SO_2 and H_2S was recorded as 11.68 mg/g and 7.96 mg/g respectively using eggshells calcinated at 900 °C. Reta G. Jalu et al. [49] prepared calcium oxide nanoparticles from eggshells using the sol–gel method of synthesis to overcome the high-temperature synthesis technique. The steps involved in the sol–gel process are shown in the Eqs. (1–3). Initially the raw eggshell powder contains calcium carbonate treated with aqueous HCl for making the uniform solution of metallic salt. After that, sol was formed by alkaline hydrolysis reaction and formation of metal hydroxide takes place. And lastly, calcined the dried powder at 900 °C for 1 h using a muffle furnace.

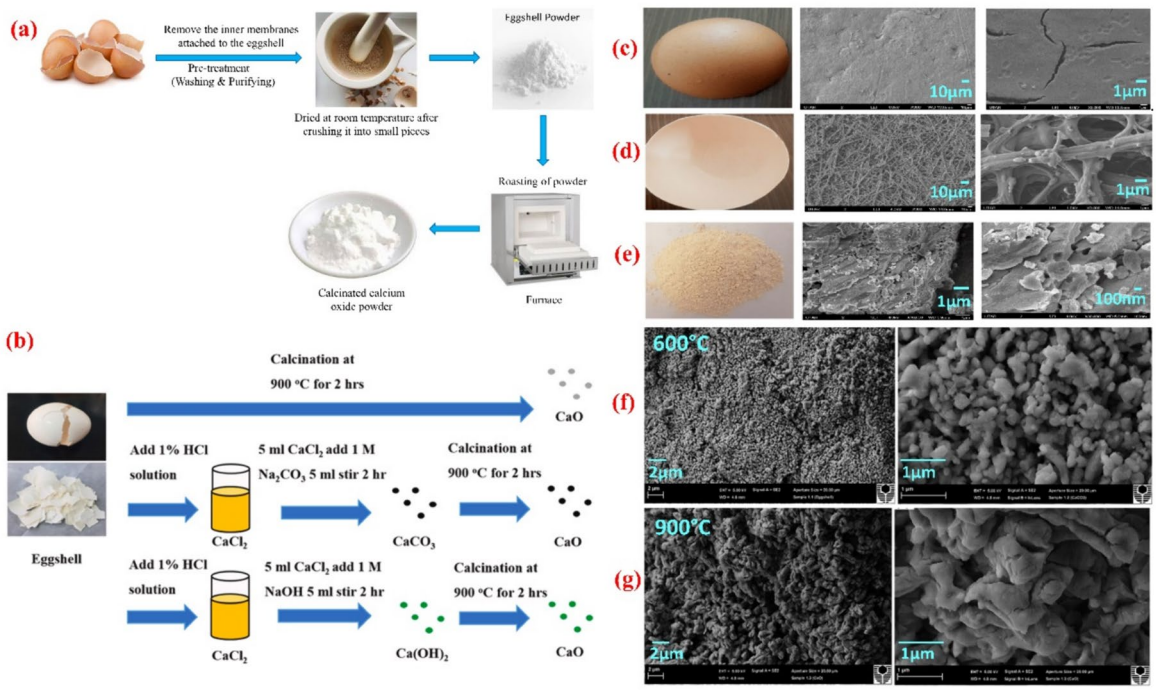

Fig. 3 Extraction of calcium oxide using eggshell (**a**) Thermal heat treatment method (**b**) sol–gel method of synthesis. [53] (**c**) FE-SEM image of an eggshell with different magnification (**d**) FE-SEM image of inner part of eggshell (**e**) Crushed eggshells powder FE-SEM image. Reproduced with permission. [48] (**f**) SEM of calcinated eggshell powder at 600 °C temperature (**g**) SEM image of eggshells calcinated at 900 °C. [180]

$$CaCO_3(s) + 2HCl(aq) \rightarrow CaCl_2(aq) + H_2O(l) + CO_2(g) \quad (1)$$

$$CaCl_2(aq) + 2Na(OH)_2(aq) \rightarrow Ca(OH)_2(s) + 2NaCl(aq) \quad (2)$$

$$Ca(OH)_2(s) + \Delta \rightarrow CaO(s) + H_2O(l) \quad (3)$$

The synthesis of calcium oxide particles from hen eggshells offers a solution to the limitations associated with bulk materials, as it demonstrates improved performance characterized by a higher surface area-to-volume ratio. This characteristic imparts size-dependent properties, such as an increased adsorption tendency, making it beneficial for large-volume wastewater treatment systems. The development of a porous structure significantly improves the performance of the synthesised calcium oxide particles. During the calcination of $Ca(OH)_2$, this structure is created as a result of the release of CO_2 and H_2O from the internal structure. Ebrahim Fayyazi et al. [50] prepared CaO catalyst derived from chicken eggshells for biodiesel production. To obtain active CaO, the researchers prepared the material at a temperature of 900 °C. To prevent contamination from CO_2 or water moisture, the calcined samples were removed from the furnace before reaching room temperature and immediately placed in a sealed glass desiccator. This ensured the preservation of the sample's integrity and minimized any undesired reactions or influences from the surrounding environment. Minglong Zhang et al. [51] conducted a synthesis of bio nano CaO by employing tea decoction to reduce the extracted CaO from chicken eggshell. This unique approach aimed to produce bio nano CaO with potential applications as a catalyst. The presence of oxygen anions on the surface of CaO plays a crucial role in its catalytic effects, particularly in transesterification reactions. CaO nanoparticles were synthesized by Lulit Habte et al. [52] using eggshell as a precursor, and the size reduction process was accomplished through the sol–gel method.

The resulting nanoparticles exhibited a mean particle size of 198 nm and displayed a spherical morphology. During the sol–gel process, the condensation reaction led to the formation of small-sized particles interconnected with each other, creating a rigid and highly crystalline inorganic network within the liquid. To enhance crystallinity, a slow addition of NaOH was employed, which promoted a low rate of nucleation and facilitated the subsequent precipitation of $Ca(OH)_2$ layers on top of one another, resulting in the formation of a highly crystalline gel. This step contributed to improving the overall crystalline structure and quality of the CaO nanoparticles. Shu-Ling Hsieh et al. [53] prepared CaO using eggshells for CO_2 gas adsorption. The method of synthesis is shown in Fig. 3(b). In addition, the researchers employed various modifiers, including amino-based polymers such as tris(hydroxymethyl)aminomethane (Tris), polyethylenimine (PEI), and polydopamine (PDA), to investigate their effects on the particle size and configuration of CaO particles. The pyrolysis of PDA resulted in the formation of relatively large pores. This can be attributed to the unique properties of PDA, which contribute to the creation of larger void spaces during the calcination process. Conversely, PEI possesses a long carbon chain structure that occupies a relatively small volume. As a result, the generated pores after calcination using PEI as a modifier are relatively small. This indicates that the size and configuration of the CaO particles can be controlled by the choice of modifier, leading to variations in pore size and overall particle characteristics.

2.2 Calcium Extraction from Sea Shells

A seashell is a hard, protective outer layer of the animal that lives in the sea. Seashell contains several layers of different microstructure having different mechanical properties. It involved a wide variety of different seashells such as mussels, cockles, scallops, and snail shells. These shells are a rich source of calcium carbonate. The synthesis of calcium oxide from sea shells is the same as eggshells the only difference in its calcination temperature. Sasiprapha Kaewdaeng et al. [54] used calcium oxide synthesized from river snail shell ash as a catalyst in the transesterification process for biodiesel production. In this research, calcium oxide was derived from the calcined river snail shell at designated temperatures (700, 800, and 900 °C) for 4 h, in a static air condition. This study identified the ideal calcination temperature as 800 °C. Utilizing snail shells as a catalyst in the reaction serves to reduce the overall expenses of biodiesel production. Moreover, this approach is linked to the capacity for recycling natural mineral resources, culminating in an ecologically mindful and sustainable process. Okorie Agwu et al. [55] showed the flowchart of the synthesis process of calcium oxide from seashells as shown in Fig. 4(a). Furthermore, it was noted that for every 1 kg of seashell subjected to calcination, a yield of 500 g (equivalent to 50% by weight) of powder was obtained. This observation aligns with the findings of Chilakala et al. [56], who reported that oyster, clam, conch, scallop, and abalone shells experienced an average weight loss of 44–46% due to the release of CO_2 gas during calcination.

Onyelowe and Onuoha (2016) also recorded similar results, noting that approximately 40.5% of the weight of snail shell was lost upon calcination. Similarly, Correia et al. [57] reported a weight loss of 40.4% for quail eggshells within the temperature range of 550–875 °C. This weight loss occurred as the shells underwent decomposition, transitioning from calcium carbonate to calcium oxide. Vivek and Sophia [58] provided a more detailed explanation for the weight loss observed during the calcination of egg and conch shells, identifying two distinct weight loss modes at

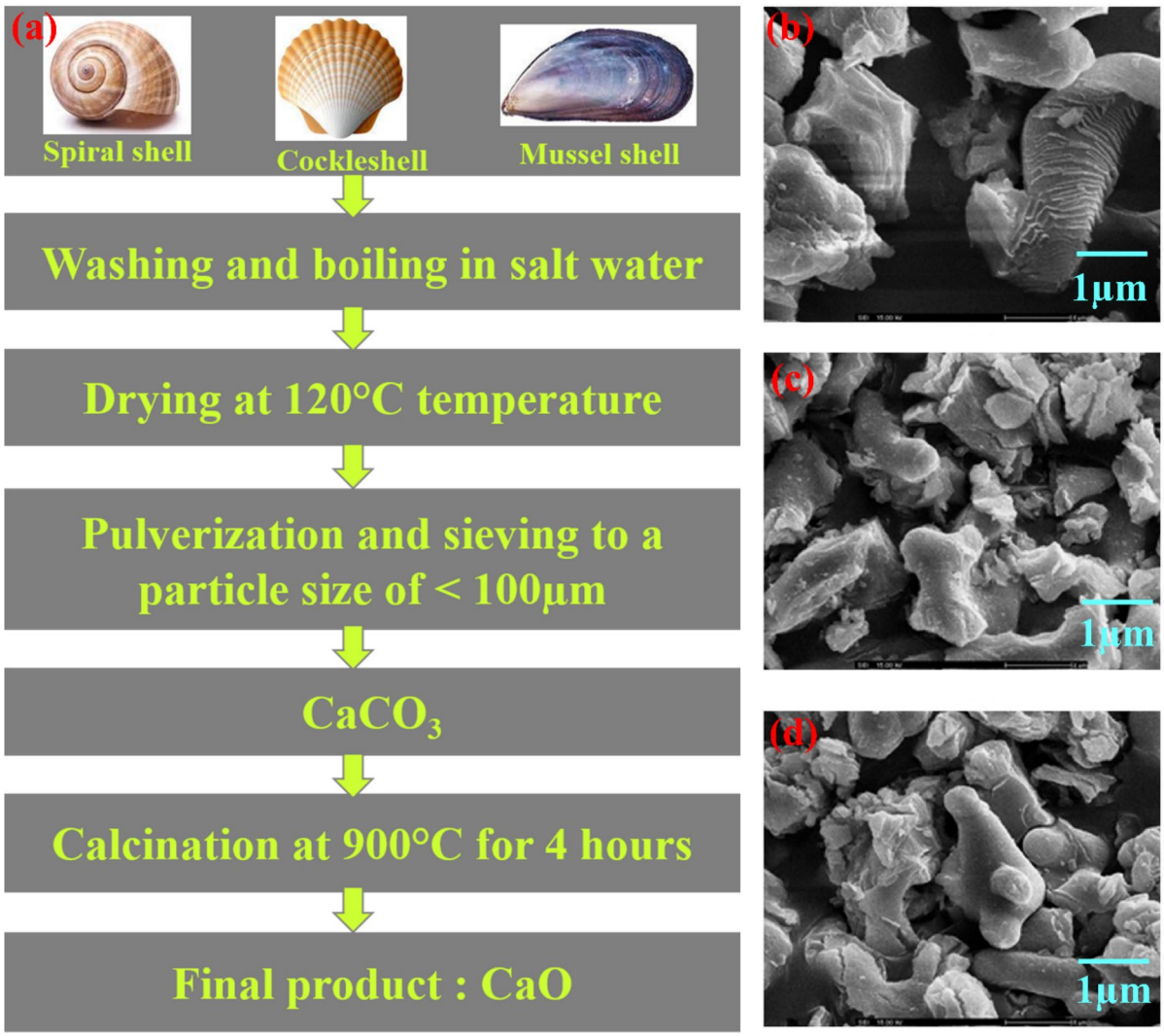

Fig. 4 (**a**) Flowchart for the obtaining of calcium carbonate and calcium oxide from sea shells. [55] SEM image of (**b**) mussel shell (**c**) cockle shell (**d**) scallop shell calcinated at 1000 degree celsius. [61]

specific temperature ranges. The first mode was characterized by a gradual and slow weight loss, occurring within the temperature range of 100–600 °C. This initial weight loss was attributed to the expulsion of water molecules and carbon oxide from the shells. The second mode was marked by a rapid weight loss, taking place between 600–800 °C. It was proposed that this sudden decrease in weight was primarily caused by the release of carbon oxide from the carbonates present within the shell structure. In a study conducted by Panu Leelatawonchai et al. [59], the extraction of calcium oxide from golden apple snail shells was investigated. The researchers observed that at a calcination temperature of 700 °C, the transformation of $CaCO_3$ phase into CaO began. Over increasing calcination time, the peak intensities of the $CaCO_3$ phase decreased, while the peak intensities of the CaO phase increased. Based on their findings, the researchers concluded that a complete phase transformation from $CaCO_3$ to CaO occurred after one hour of calcination at 800 °C. In a study conducted by Ikbal Bahar Laskar et al. [60], calcium oxide catalysts were derived from snail shells for biodiesel production. Initially, the snail shells underwent a sequence of drying and grinding stages. Subsequently, they were subjected to calcination within a muffle furnace for a duration of 4 h, spanning a temperature spectrum from 400 °C to 1000 °C. Following the calcination process, the resultant catalyst was meticulously placed in a desiccator to shield it from air exposure. The research findings indicated that when exposed to a temperature of 1000 °C, a remarkably pure form of calcium oxide, with a purity level as high as 97.14%, was attained. Furthermore, the researchers noted that calcination at 900 °C led to the creation of unevenly sized semi-spherical particles characterized by

porous exteriors. The presence of this porosity on the catalyst's surface played a substantial role in augmenting the BET surface area, thus significantly elevating its catalytic efficiency. Achanai Buasri et al. [61] synthesized calcium oxide using a variety of shells such as mussel, cockle, and scallop shells by simple calcination method at a calcination temperature ranging from 700 °C to 1000 °C for 4 h holding time. The derived calcium oxide from the mussels, cockles, and scallops gives purity of 98.367%, 99.170%, and 97.529% respectively, and the SEM images of all three shells are shown in Fig. 4(b-d). All the shells showed almost the same kind of morphology as observed by SEM. The calcined waste shells were irregular in shape, and some of them bonded together as aggregates. According to the BET analysis, the mussel shell exhibited notable distinctions in surface area (89.91 m^2/g) and pore volume (0.130 cm^3/g) in contrast to the cockle and scallop shells (which recorded values of 59.87 and 74.96 m^2/g; 0.087 and 0.097 cm^3/g, respectively). In a notable study conducted by Reddy et al. [62], revealed that employing a 20 nm-sized CaO catalyst with a surface area of 90 m^2/g could yield an impressively high biodiesel rate of 99% at ambient temperature. This outcome was contrasted with the usage of a commercial CaO catalyst, which possessed a markedly smaller surface area of 1 m^2/g, leading to a considerably diminished yield of 2%.

2.3 Silica Extraction from Rice Husk

Rice husk is a major source of silica production. When rice husk is burnt, it produces rice husk ash. Rice husk ash is an environmental waste, which contains 60–80% of amorphous silica depending upon the type of rice. There are various methods reported for the extraction of silica from rice husk as shown in Fig. 5(a): (i) Acid leaching method: this method involves treating rice husk ash with any one of acids HCl, H_2SO_4, and HNO_3 to dissolve the silica. The silica is then precipitated by adding a base such as sodium hydroxide (ii) Alkali fusion method: in this method, rice husk is mixed with a strong base such as sodium hydroxide and heated at high temperatures to form a molten mass. The molten mass is then cooled and dissolved in water to extract the silica (iii) Sol–gel method: this method involves

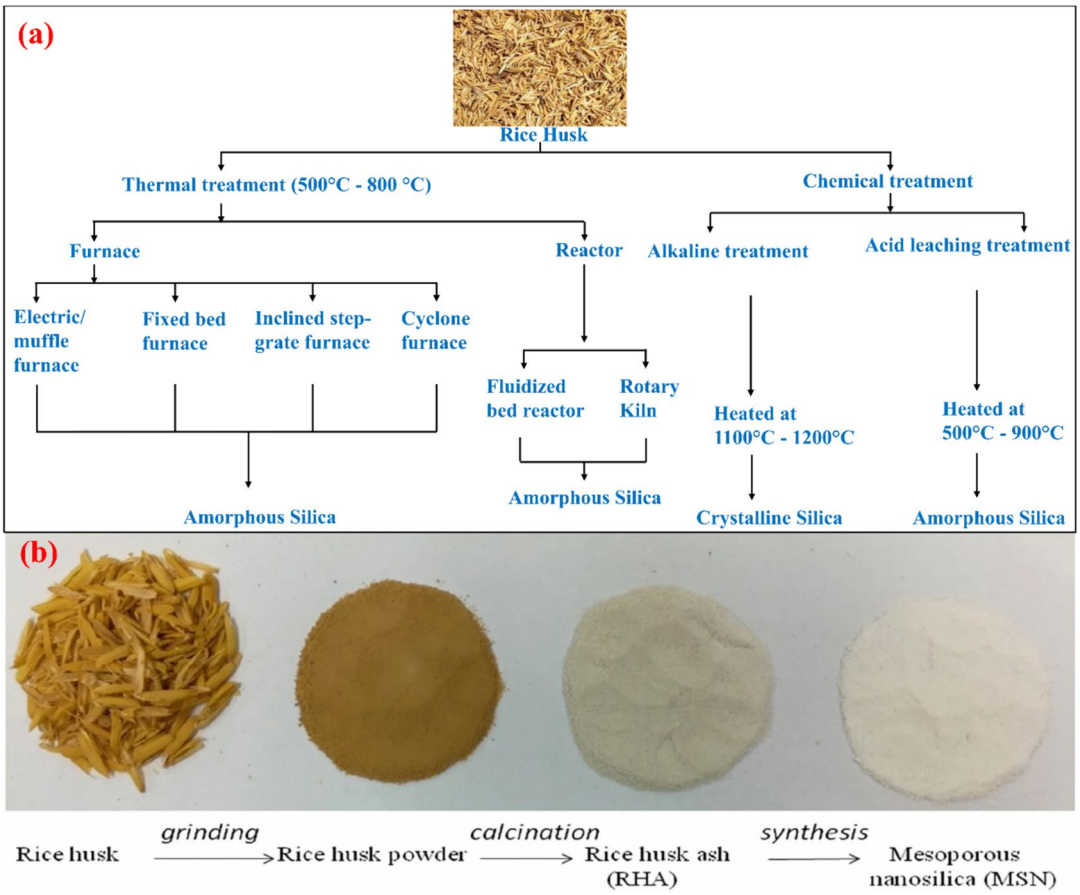

Fig. 5 (**a**) Various method of synthesis for the extraction of silica from rice husk [181] (**b**) Different physical transformations occurred during the conversion of rice husk into silica nanoparticle. [67]

dissolving the rice husk ash in an acid solution to form a sol. The sol is then heated to form a gel, which is dried and calcined to obtain pure silica. Each of these methods has its own advantages and disadvantages in terms of efficiency, cost, and environmental impact. The choice of method will depend on the specific requirements of the application and the availability of resources. In the process of generating bio-silica from rice husk via the hydrothermal method, steam is commonly employed within a pressure spectrum of 50 to 250 bar, alongside temperatures spanning from 200 to 400 °C. [63] This process includes biomass fragmentation and thermal decomposition, resulting in the generation of predominantly liquid products and hydrochar. The hydrochar still retains silica content, which can be further extracted. However, this particular route has certain drawbacks that limit its attractiveness. The operation requires a significant amount of energy, while the energy produced is relatively low. Additionally, the ash obtained from the process contains a high proportion of unburnt carbon content (UCC) due to incomplete oxidation. These factors contribute to the downstream processing of the product being costly. Ji Yeon Park et al. [64] prepared biocompatible silica nanoparticles from three different routes such as combustion, acid leaching, and alkali extraction. In the combustion process, they did direct calcination of rice husk at 900 °C temperature. In the acid-leaching process, firstly treated with H_2SO_4 and then dried and calcinated at 900 °C. In the alkali extraction process, initially, rice husk was treated with NaOH solution and during the reaction, silica dissolved into the solution, and the liquid friction was filtered out with filter paper. The second step is to adjust the pH neutral by adding acetic acid, and silica nanoparticle precipitate. Again, calcinated at 900 °C followed by drying. During the bio-compatibility assay, it was observed that the acid-leached nanoparticles (NPs) exhibited higher toxicity compared to the alkali-extracted NPs, despite being purer in composition. The toxicity of the combustion and acid-leached NPs is attributed to the generation of oxidative radicals, which can potentially cause DNA damage [65]. They conclude that the alkali extraction process is the most effective method to increase the biocompatibility of the material. Ikram Ul Haq et al. [66] studied the effect of NaOH concentration, the effect of extraction time, and the effect of the ratio (Moles of NaOH/Grams of RHA) under various reflux conditions on the extraction of silica. They followed the sol–gel method of synthesis by treating rice husk ash with aqueous NaOH for various time periods and later acidified with H_2SO_4 to form a white gelation. They reported that the silica yield is negligible at 0.4 mol/L of NaOH concentration and it continuously increases up to 1 mol/L after that it becomes saturated. Additionally, the researchers examined the extraction time and noted that the percentage yield of the extracted silica increased as the extraction time was prolonged, up to a duration of 90 min. However, beyond this point, the yield of silica remained relatively constant and did not show significant further increase with longer extraction times. Deivaseeno Dorairaj et al. [67] utilized an alkaline extraction (NaOH) followed by acid precipitation method to treat rice husk and obtain high-purity rice husk ash (RHA) with a silica content exceeding 98% by weight. The sol–gel synthesis technique was employed for this purpose. In this process, the alkaline extraction of rice husk resulted in the dissolution of silica in an alkaline medium with a pH level above 10, forming a sodium silicate solution with a pH level exceeding 12. The subsequent hydrolysis and condensation reactions occurred simultaneously, leading to the transformation of the sodium silicate sol into a polymeric gel network. During this transformation, hydrochloric acid (HCl) acted as a catalyst, facilitating the precipitation of silica from the gel network [68]. In their findings, it was determined that the average pore size of the synthesized silica nanoparticles was 8.5 nm, indicating that they possessed a mesoporous structure. The BET specific surface area was measured to be 300.2015 m^2/g, and the pore volume was found to be 0.659078 cm^3/g. These parameters highlight the porous nature of the nanoparticles.

Figure 5(b) illustrates the different physical transformations that occurred during the conversion of rice husk into white mesoporous silica nanoparticles. According to Real et al. [69], it was found that performing acid leaching on rice husks prior to burning resulted in the production of silica powder with a significant surface area. However, when the acid leaching stage was conducted after the combustion process, the resulting silica surface area was not as high. Kalapathy et al. [70] employed a sequential extraction method to obtain silica from rice husks. The procedure started with a leaching stage to remove impurities, then the silica was dissolved by adding NaOH, creating a sodium silicate solution. Afterwards, the sodium silicate solution was treated with hydrochloric acid (HCl) to precipitate the silica. The precipitated silica was then dried at a temperature of 800 °C for a duration of 12 h, resulting in silica with an approximate purity of 91%. However, 4% of the sodium impurities were still present in the extracted silica, necessitating a washing step to bring the sodium concentration down to less than 0.10%. Unfortunately, this supplementary washing process extends the overall procedure and reduces its efficiency. To tackle this problem, Kalapathy et al. [71] developed a method aimed at reducing sodium impurities in extracted silica without the need for additional washing steps. In their previous research, they found that when obtaining silica at an alkaline pH, a washing stage was required after drying the aqua gel. However, their newly devised method, described in this study, eliminated the necessity for such washing steps. The goal of the study was to synthesise sodium silicate as silica at pH 4 by adding sodium silicate to a solution that also contained

hydrochloric acid, oxalic acid, or citric acid. They examined the purity of the silica made at pH 4 to that produced at pH 7, which was accomplished by mixing an acid solution with a sodium silicate solution. The findings revealed that at pH 4, gelation occurred at a slower rate, allowing for the rapid diffusion of sodium ions out of the gel matrix. As a result, the silica extracted at pH 4 exhibited lower sodium content compared to that extracted at pH 7, where rapid gelation trapped sodium ions within the gel matrix. Furthermore, compared to silica precipitated with hydrochloric acid, silica deposited using citric and oxalic acids to create sodium silicate resulted in lower sodium levels. The different particle sizes of the sodium salt were thought to be the cause of this variation. Due to the sodium chloride's small size, it was able to adhere to the surface of microporous silica, making it difficult to wash away and raising the sodium levels. Silica obtained within the pH range of 4 to 7 demonstrated a purity range of 89–91% with an average water content of 2.30%. According to Liou et al. [72], the surface area of the extracted silica is significantly influenced by the acid treatment method employed. The study investigated the precipitation of silica in a sodium silicate solution using hydrochloric acid (HCl), sulfuric acid (H_2SO_4), oxalate acid ($C_2H_2O_4$), and citric acid ($C_6H_8O_7$). The findings revealed that the silica precipitated with citric acid exhibited the lowest surface area, while silica obtained through sulfuric acid or oxalic acid precipitation showed an increase in surface area. The maximum surface area was observed when silica was precipitated using hydrochloric acid. The acid sequence, ranked from the largest to the smallest surface area, was HCl, H_2SO_4, $C_2H_2O_4$, and $C_6H_8O_7$. The size of the salt used played a role in the trapping of the salt within the gel matrix, which hindered its removal during washing and resulted in reduced surface area coverage. Thus, hydrochloric acid was identified as the optimal acid for silica precipitation. The study also investigated the effect of gelation pH variations from 1 to 11 on the surface area of the silica. The surface area of the silica exhibited a strong dependence on pH, with decreasing pH leading to an increase in surface area. Gelation did not occur at pH values below 3, and at pH 3, solid settling commenced while gel formation was slow. The optimum yield was achieved at a pH level of approximately 7, with pH values exceeding 8 causing unstable gel formation and partial dissolution. The gel almost entirely dissolved at pH 11. Additionally, the porosity and particle size of the resulting silica were significantly influenced by the gelation's pH. Due to the promotion of polycondensation reactions aided by OH- during the gel formation process, increasing pH from 3 to 7 resulted in larger particle size and increased porosity. In acidic conditions, reducing the pH of gelation converted siloxane bonds (Si–O-Si) to silanol bonds (Si–OH), leading to slower gel formation. In such cases, the silica consisted of smaller primary particles, resulting in a larger surface area. In summary, the formation of surface silanol and siloxane bonds contributed to the repulsion of particles, leading to an increase in electrostatic repulsion [73]. The catalytic effect on charged particles promotes their further growth, leading to an augmented particle size as pH increases. Consequently, this phenomenon induces an increase in porosity and a decrease in the surface area of the sample. Pa and Kein [74] tested different acid concentrations (0.1, 0.5, and 1 mol/L), leaching times (1–3 h), and leaching temperatures (70, 80, and 90 °C) in an effort to determine how well rice husks would react to the use of oxalic acid. The leached rice husks were then calcined for three hours at 800 °C. As a result, with higher acid concentration, longer leaching time, and higher leaching temperature, the silica content in the ash increased from 92.4% to 99.3%. Furthermore, when rice husks were subjected to acid leaching using 2 mol/L HCl at 90 °C before calcination at 700 °C, the silica content in the ash reached 99.74%. Similarly, Mehdinia [75] employed a method involving the use of 3% HCl and H_2SO_4 for acid leaching of rice husks at 105 °C for 2 h. The leached rice husks were subsequently calcined at 800 °C for 4 h. In this process, the silica content in the resulting ash was determined to be 94.24%. Bakar et al. [76] conducted a study to investigate the effect of acid leaching on the silica content and surface area of rice husk ash produced through calcination at temperatures ranging from 500 °C to 900 °C. Without acid leaching, the silica purity and surface area were found to be 95.77% and 118 m^2/g, respectively. However, with HCl and H_2SO_4 leaching, the silica purity increased to 99.08% and 99.58%, while the surface area increased to 218 m^2/g and 208 m^2/g, respectively. Wenwen Guo et al. [77] presented a straightforward and effective heat treatment method combined with acid leaching for extracting silica from rice husk. They determined that the optimal calcination temperature was 600 °C, with a holding time of 3 h, which successfully eliminated the organic matter present in the rice husk. This process yielded a purity of 99.45% with a 21.7% extraction yield. In another study, Ghosh and Bhatta cherjee utilized H_2SO_4 for acid leaching, followed by extraction at NaOH concentrations of 0.5, 1, and 1.5 mol/L for 1 h. They achieved a silica recovery rate ranging from 95 to 98% with a surface area of 150–200 m^2/g.

2.4 Silica Extraction from Sugarcane Bagasse

Bagasse, despite being categorized as waste, holds significant potential as a sustainable and environmentally friendly resource, offering valuable contributions to sustainable development and technological advancements. Both sugarcane bagasse and rice husk contain significant amounts of silica but the extraction of silica from sugarcane bagasse is a complex process that requires careful handling of chemicals and equipment because the chemical composition of

the sugarcane bagasse is more complex than rice husk [78]. It contains a variety of organic and inorganic compounds, including lignin, hemicellulose, and cellulose, which can interfere with the extraction process. Sugarcane bagasse particles are generally larger than rice husk particles, which makes it more difficult to extract silica. Larger particles require more energy and time to break down and extract the silica. It typically requires pre-treatment and more aggressive acid conditions to remove impurities and other unwanted materials. But still, various reports are available for the synthesis of silica from sugarcane bagasse. To remove the residual metallic impurities, researchers follow pre-treatment method such as acid leaching due to it being a cost-effective and faster breakdown of complex compositions make it an efficient method. Acid leaching is required to remove the high impurity content and retain the biogenic structure of silica with high purity. According to Worthanakul et al., the silica content composition of SCBA is approximately 89.04%. In a separate study by Baharudin and Santhanam [79], SCBA was subjected to controlled temperature pyrolysis at 600 °C for 4 h, resulting in a SiO_2 content of approximately 70.97%. Additionally, Drummond et al. (1996) compared the yield of silica from different preparations of sugarcane bagasse ash: natural burning (SCBA-NB) and laboratory burning (SCBA-LP) at 700 °C in a muffle furnace for two hours, followed by alkaline extraction. The study showed a slightly different yield, with approximately 94.47% silica obtained from natural burning and 96.93% silica obtained from laboratory burning. Among the various acids investigated for leaching self-compacting concrete (SCBA), sulfuric acid (H_2SO_4) is the most widely utilized leaching agent. However, alternative acids, including hydrochloric acid (HCl), hydrogen fluoride acid (HF), nitric acid (HNO_3), and phosphoric acid (H_3PO_4), have also been explored for this purpose. Norsuraya et al. [80] reported that the silica content in sugarcane bagasse composition was 53.1% prior to HCl acid leaching. However, after undergoing leaching with HCl, the silica content increased significantly to 88.13%. Additionally, Luyza Bortolotto Teixeira et al. [81] explored three distinct routes for synthesizing silica from sugarcane bagasse. In Route A, bagasse ash was directly subjected to calcination without any pre-treatment. As the temperature increased from 500 °C to 700 °C, the obtained purity ranged between 43.6% and 52.1%. On the other hand, Route B and Route C involved pre-treatments such as acid leaching or thermal treatment. In a different study conducted by G. Falk et al. [22], silica nanoparticles were synthesized using two different methods: the sol–gel method (method 1) and thermal treatment (method 2), followed by acid leaching with leached sugarcane bagasse. Thermogravimetric analysis (TG/DTA) indicated that method 1 exhibited a higher mass loss compared to method 2. The specific surface area values obtained through the BET method were 124.89 m^2/g for the silica prepared using method 1 and 8.28 m^2/g for the silica prepared using method 2, with respective pore diameters of 14 nm and 2 nm. Notably, the material prepared via the sol–gel method demonstrated superior results in terms of specific surface area, porosity, pore volume, and average pore diameter compared to the material obtained through direct calcination. Consequently, the materials obtained using method 1 (sol–gel) exhibit greater potential for utilization as adsorbent materials. S. Rovani et al. [82] successfully prepared silica nanoparticles with a remarkable purity exceeding 99%. They employed cetyltrimethylammonium bromide (CTAB) as a stabilizer and size controller to regulate the particle size. The synthesis process involved pre-treatment with HCl and NaOH to form a Na_2SiO_3 solution. The silica nanoparticles that emerged demonstrated exceptional purity and showcased dimensions spanning from a few micrometers to under 20 nm. Furthermore, they featured a distinct surface area of 131 m^2/g. In a study by Vaibhav et al. [83], they successfully produced 98% pure silica from waste materials through alkali/acid treatment. Initially, the waste materials underwent moisture removal on a hot plate and were sintered at 900 °C for 7 h. The resulting sintered powder was then subjected to a two-step treatment process. First, it was treated with 1 M NaOH to form sodium silicate, and then with 6 M H_2SO_4 (maintaining a pH of 11.8) to precipitate silica. Following the acid extraction process, a high purity of 98% (wt%) SiO_2 was achieved, with yields of 78% from rice husk, 71% from sugarcane bagasse, and 52% from bamboo leaves. In a separate study, bagasse dissolution was carried out using alkaline NaOH, followed by precipitation with sulfuric acid. Analysis using energy-dispersive X-ray spectroscopy (EDAX) revealed the presence of impurities such as potassium, calcium, and magnesium, resulting in 77% pure silica. Additionally, the researchers investigated the silica content in bagasse through thermal treatment at different temperatures: 500 °C, 600 °C, and 700 °C. As a result, ash with purities of 12.65%, 10.89%, and 9.95% respectively, were obtained. XRF analysis revealed that the silica levels in the bagasse ash increased in a sequential order corresponding to the experimental temperatures, with values of 76.168%, 76.292%, and 77.286%, respectively. In their study, Prinya Chindaprasirt et al. [84] carried out the dispersion of sugarcane ash in 1 M NaOH, using different ash-to-base ratios of 1:5, 1:8, and 1:10 (w/v). The resulting mixture was heated to 90 ± 5 °C and stirred using a magnetic stirrer for 1 h. Subsequently, the mixture was allowed to cool to room temperature. The ash residue was then separated through filtration, and the filter cake was washed with hot water, using a volume twice that of the NaOH solution used. The resulting filtrate contained sodium silicate, along with the washing water. To adjust the pH to 7, 2.5 M HCl was added to the filtrate, and the mixture was left to age at room temperature for 24 h to allow for silica maturation. The silica

was then filtered and washed with hot water before being dried at 100 ± 5 °C for 5 h.

2.5 Silica Extraction from Coconut Husk

The coconut husk is a highly rough exterior shell of a coconut. It contains a high amount of lignin and phenolic content which is why the husk is very elastic and durable in nature. Coconut husks are versatile and sustainable material with a wide range of uses as a biofuel and can be burned to produce energy. Coconut husks contain high levels of silica, particularly in the form of silicon dioxide (SiO_2). Muhammad Fahmi Anuar et. al [85]. explored the waste coconut husk to extract silica using two different methods (i) acid treatment (ii) alkali treatment. In the acid treatment method, the coconut husk ash was leached with sulphuric acid at 50 °C temperature and dried in a hot air oven to get powdered silica. In the second method, the coconut husk ash was treated with 2.5 N NaOH to obtain a sodium silicate solution. After filtration, the sodium silicate solution was treated with sulphuric acid to get white precipitated silica by adjusting the pH of the solution. They conclude that after the chemical treatment, the percentage of silica obtained effectively increased from 9.24% to 91.76%. The FE-SEM image of the sample prepared after various calcinated temperatures and after acid treatment are shown in Fig. 6(a-d). M. Z. Norul Azlin et al. [86] also reported silica extraction from coconut husk using an acid treatment method with 5 N sulphuric acid and in alkali treatment, ash was leached with 2.5 N NaOH followed by 5 N sulphuric acid. They reported that after acid treatment and alkali treatment, the yield comes out to be 61.92% and 75.58% respectively.

3 Structural Properties of Calcium Silicate Material

The general formula of calcium silicate is $CaSiO_3$. Di-calcium silicate and tri-calcium silicate with the basic formula Ca_2SiO_4 and Ca_3SiO_5 respectively are also well-known calcium silicates [87]. The theoretical composition of CaO and SiO_2 in $CaSiO_3$ is 48 wt % and 52 wt % respectively. [88] Calcium silicate typically contains fewer toxic elements like magnesium, iron, titanium oxide, and manganese due to its natural formation process and the geological conditions under which it is produced. CS is a contact metamorphic deposit between limestones and igneous rocks with garnet, diopside, calcite, and quartz as common constituents. It is a polymorphic substance with two forms: at low temperatures, it is found in a triclinic and monoclinic form known as para-wollastonite (β wollastonite), and at high temperatures, it exists in a pseudo-hexagonal form known as pseudo-wollastonite (α wollastonite) [89, 90]. Usually, wollastonite is found in a para-wollastonite state but at 1125 °C temperature para-wollastonite is transformed into the pseudo-wollastonite form [91]. Fig. 7 shows the wollastonite-1 T form along with β-wollastonite and α-wollastonite. Wollastonite-1 T and β-wollastonite are closely related and occur together because of their small structural energy difference but they crystallize in triclinic and monoclinic structures respectively. The β-wollastonite is a chain silicate and its structure consists of an infinitely long single chain as shown in Fig. 7(c) along the b-axis. The unit cell constant of wollastonite-1 T is a = 7.079, b = 7.3309, c = 7.938, α = 103.41°, β = 95.30°, γ = 90.07 and space group P1, β-wollastonite belong to P21/a space group and unit cell constant is a = 15.409°, b = 7.322°, c = 7.066°, α = γ = 90°, β = 95.30, for α-wollastonite unit cell constant is a = 6.8394, b = 11.8704, c = 19.6313, α = γ = 90°, β = 90.667 with space group C2/c. [92]

4 Synthesis of Calcium Silicate and its Derivatives

Various preparation techniques are available for the synthesis of CS material, such as the co-precipitation method [93], solid-state reaction technique [94], sol–gel method [95, 96], hydrothermal process [97], ultrasonication technique, etc. The solid-state reaction takes a long time and requires a high calcination temperature because of limited diffusion during the calcination but it is still the most used and important method due to the occurrence of natural CaO and SiO_2 in abundant form. While co-precipitation, sol–gel, and hydrothermal methods require less calcination temperature with controlled morphology and homogenous composition.

The sol–gel synthesis techniques can opt for the various nanostructure, especially metal oxide nanoparticles. In this method, metal hydroxide reacts with either water or alcohol to form the sol through continuous heating and stirring by the hydrolysis process. After the transformation occurs from the colloidal suspension of sol to the 3D interconnecting network of gel [98]. Since the gel formed is wet there is a proper way of drying the gel and getting the powder. If it is an alcoholic solution then drying is done by burning the alcohol. In this process, the size of the particle is controlled by the precursor concentration, calcination temperature, and the pH value of the solution [99]. The concentration of precursor and dispersant in the sol–gel method also influences the size and shape of the nanoparticle. Spheroid shape CS nanoparticle with an average grain size of 50–60 nm is obtained by using the HNO_3, CH_3COOH, H_2O, and PEG200 as a dispersant. The reaction temperature and holding time also contribute to controlling the homogenous shape and size of the particles. Wet chemical synthesis technique is more effective for the synthesis of selective surface structure, phases, shape, and size [100]. In this process we can

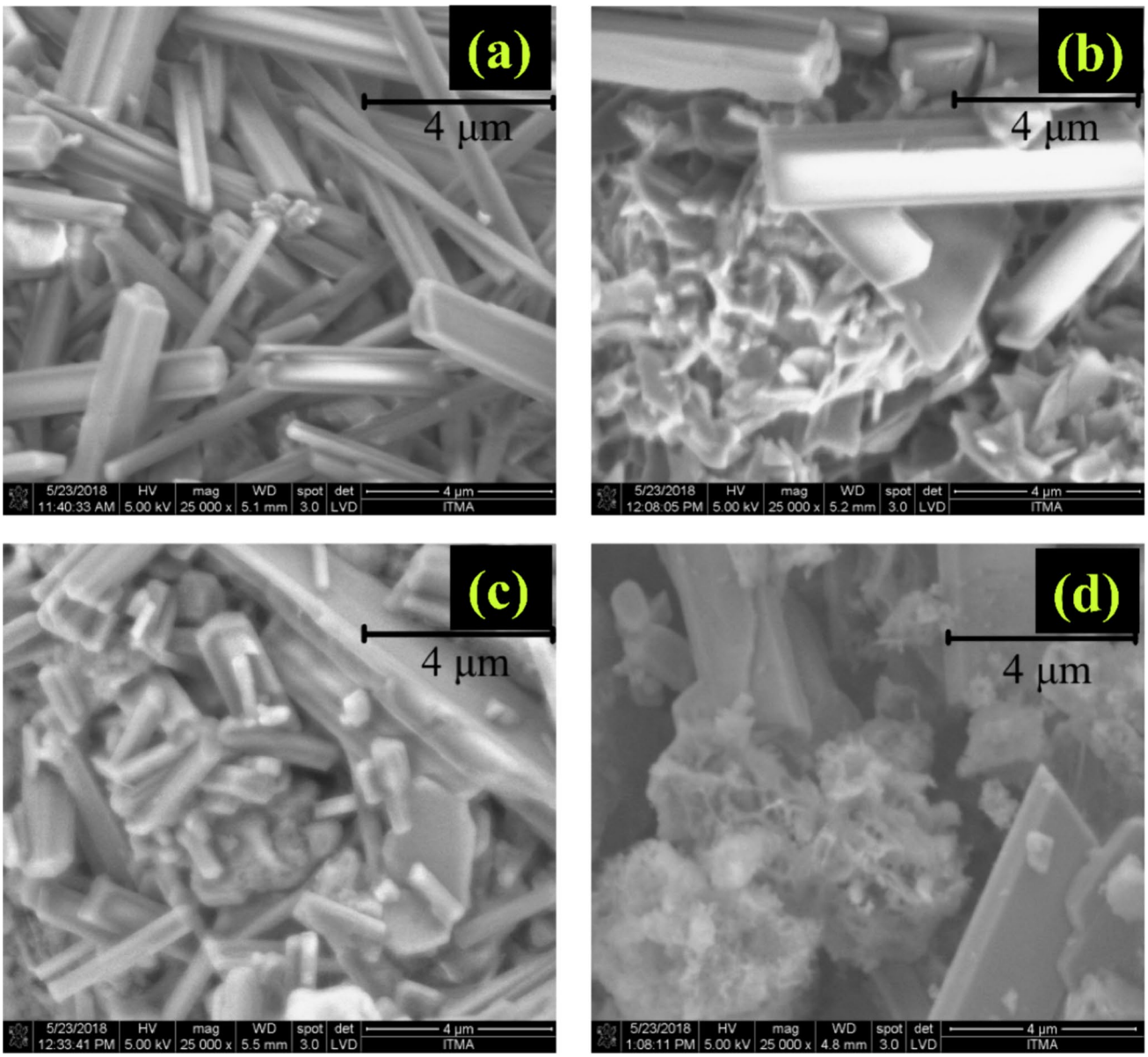

Fig. 6 FE-SEM of coconut husk ash calcinated at (**a**) 500 °C (**b**) 600 °C (**c**) 700 °C (**d**) after acid treatment. [182]

tuned the reaction kinetic and thermodynamic condition by changing the pH value, calcination temperature, additives or surfactant, heating and cooling rate, type of ligands, and concentration of the substance to get the desired morphology. The type of surfactant decides the particle size and reduces the agglomeration in the solution [101]. CS nanoparticles with particle size 40 nm were prepared by controlled addition of 0.5 mol sodium silicate to 0.5 mol calcium nitrate tetrahydrate using the ammonia surfactant with pH adjusted to 11.4 [102]. Mesoporous CS is synthesized by wet chemical synthesis followed by an acid modification technique to create meso-porosity. Hydrochloric acid treatment was employed to adjust the pH of the solution and induce mesoporosity in CS particles, resulting in pore diameters of up to 4–5 nm. The mesoporous structure was achieved by subjecting the synthesized CS particles to acid modification using hydrochloric acid at pH 7, 4.5, and 0.5. As a result of this acid modification, the BET specific average surface area significantly increased. Specifically, the surface areas were enhanced to 221 m^2/g, 333 m^2/g, and 356 m^2/g at pH 7, 4.5, and 0.5, respectively, whereas the unmodified CS particles exhibited a surface area of 65 m^2/g [103]. CS nanowires of diameter 10–30 nm are synthesized by the simple and cheap hydrothermal route without using any template and surfactant. The hydrothermal method controlling the morphology of the material requires either by

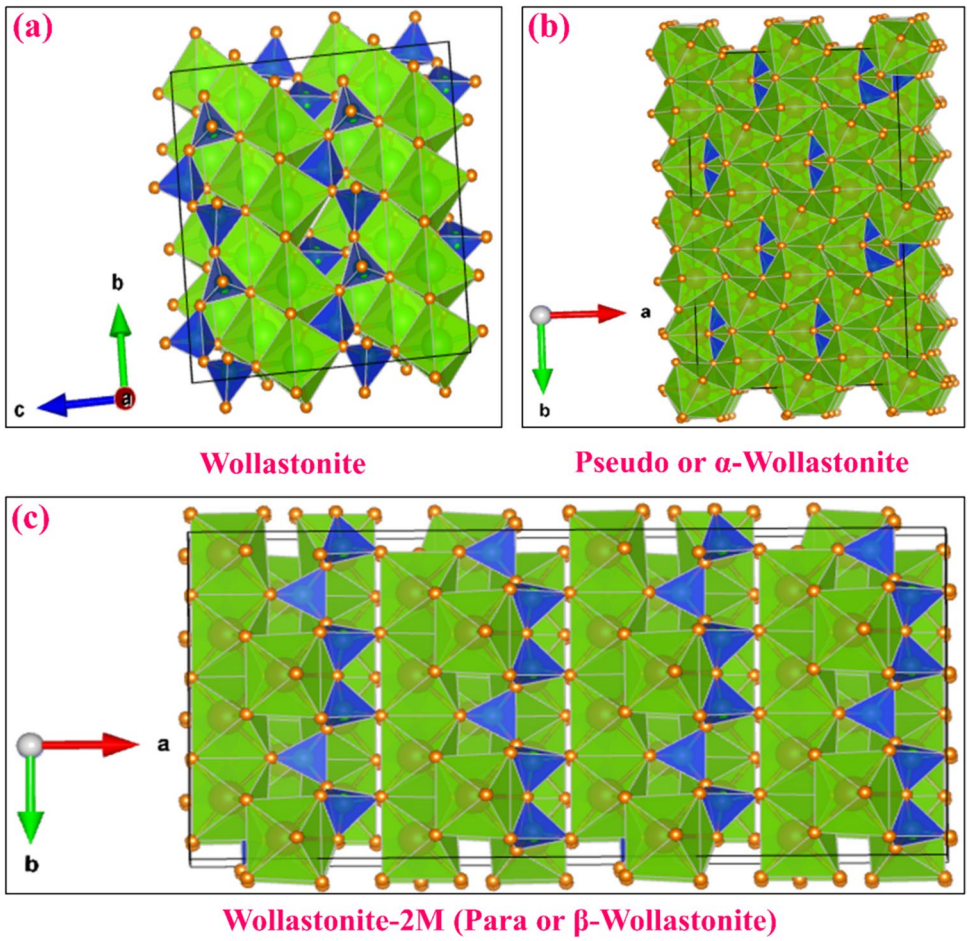

Fig. 7 Crystal structure of (**a**) Wollastonite-1 T (**b**) Pseudo or α-Wollastonite (**c**) Wollastonite-2 M (Para or β-wollastonite). Small red spheres represent oxygen atoms, blue tetrahedra are (SiO4)2- and green polygons are Ca cation sites

low pressure or high pressure depending on the vapor pressure of the main composition [104]. Growth time and temperature also play an important role to optimize the diameter of the nanowires. L.Z.Pei [105] showed that by decreasing the hydrothermal temperature the diameter of the nanowire decreases up to 20–100 nm. The hydrothermal reaction was applied to synthesize β-$CaSiO_3$ nanowires. Xonotlite nanowires, ranging in diameter from 50 to 100 nm, were successfully synthesized by Li and Chang [106] using tetraethyl orthosilicate (TEOS) and $Ca(OH)_2$ as the precursors. The hydrothermal method was employed, and in this process, cetyltrimethylammonium bromide (CTAB) was utilized as the template for nanowire formation. Tobermorite nanowires, with a diameter of 20–30 nm, were synthesized by Lin et al. [107] using a hydrothermal microemulsion method. By subjecting xonotlite or tobermorite nanowires to calcination at 800 °C, β-$CaSiO_3$ nanowires could be obtained. However, these methods involved the use of templates or organic solvents, which can be harmful to both health and the environment. In an alternative approach, β-$CaSiO_3$ nanowires were successfully synthesized from $Ca(NO_3)_2$ and Na_2SiO_3 as the starting materials, without the need for any templates or surfactants. This method eliminates the use of harmful substances and promotes a safer and more environmentally friendly synthesis process [104]. Certainly, the inclusion of additional templates, surfactants, Si^{4+} ions, or [NO_3] in the synthesis system undoubtedly leads to increased costs and a more intricate purification process. Furthermore, it can potentially result in a higher degree of pollution in the final product, which is highly undesirable.

Recently CS derived from biomass is a cost-effective and environmentally friendly concept. Rimruthai Phuttawong et al. [108] employed a solid-state reaction method to synthesize calcium silicate (CS) using rice husk and snail shell (Pomacea canaliculata) as raw materials. Rice husk and snail shells have high silica (SiO_2) and calcium oxide (CaO) contents, with percentages of 91.50% and 98.25%, respectively. The researchers mixed the shell and rice husk powders in a 1:1 molar ratio and subjected them to milling for varying durations to optimize the production of high-purity CS. Through their optimization process, it was determined that a milling time of 8 h, a calcination temperature of 1000 °C, and a holding time of 2 h were suitable for the synthesis of CS. Interestingly, the X-ray diffraction (XRD) pattern of CS exhibited no change in structure with increasing milling time. However, the intensity of the XRD peaks increased as

the milling time prolonged, suggesting that the milling time had no impact on the phase transformation of CS. The scanning electron microscopy (SEM) analysis revealed that higher calcination temperatures yielded smaller and more uniform particles. The average particle size obtained was less than 10 µm. F.H.G. Leite et al. [94] reported CS synthesis using avian eggshells (source of calcium) and chamotte (source of silica). They obtained a CS by using a molar ratio of eggshells and chamotte is 1:1, 2 h milling time, and 1100 °C calcination temperature with a holding time of 24 h. Along with CS, minor amounts of larnite and rankinite were also observed in XRD characterizations. Heriyanto et al. [17] proposed a method of synthesis of CS using 100% waste materials. They reported that 75% of waste glass and 25% of seashell combination gives better results at 1200 °C calcination temperature. Through an increase in temperature to 1200 °C, a pseudo-wollastonite material with a smoother surface was successfully obtained, exhibiting an acicular crystal structure at the fracture surface. As the processing temperature was elevated, greater levels of shrinkage were observed, accompanied by smoother surfaces. The measured shrinkage values for the samples were 15%, 22%, and 28%, respectively. The resulting calcium silicate exhibited a distinctive needle-shaped structure. Manmeet Kaur Chhina et al. [109] derived samarium-doped di-calcium silicate from agro-food waste using a solid-state reaction method. They homogenized ground the stochiometric amounts of eggshell, rice husk, and Sm_2O_3 for 2 h in an agate mortar. Further they did calcination at 1250 °C temperature for 4 h to obtain phosphor material. The optical band gap of these phosphors was determined to be within the range of 3.56–3.67 eV. In addition to the samarium (Sm) photoluminescence (PL) emission bands, the researchers also observed emission bands from titanium (Ti) ions, which were present in the agro-food waste used. The inclusion of TiO_2 in the Ca_2SiO_4 host made it optically active, resulting in a shift of the emission region of the phosphors towards a bluish-green hue. Consequently, it can be concluded that the presence of agro-food waste enhances the optical properties of the material, offering improved performance in terms of its optical emission. In a comparative study conducted by Srinath Palakurthy et al. [110], the synthesis of calcium silicate ceramic from biowaste resources was investigated using a sol–gel method. Two different approaches were employed: (i) a chemical route using calcium nitrate tetrahydrate ($Ca(NO_3)_2{\cdot}4H_2O$) and tetraethylorthosilicate (TEOS) as precursors, referred to as CCS, and (ii) a green synthesis route utilizing rice husk and eggshells, referred to as NCS. The in-vitro behavior of these materials was examined. Through TG–DTA analysis, it was determined that the NCS exhibited a lower crystalline temperature compared to the CCS. In terms of in-vitro bioactivity, the results revealed that the apatite crystals formed in the NCS route were densely packed and demonstrated a faster growth rate compared to those in the CCS. Moreover, the peak intensities of the NCS powder were slightly higher than those of the CCS, indicating a better level of crystallization for the calcium silicate synthesized from rice husk ash (RHA) and eggshell materials. The average crystallite size was calculated to be approximately 48.3 nm for NCS and 62.8 nm for CCS. Maroua H. Kaou et al. [111] derived calcium silicate from the combination of eggshells and silica gel using a solid-state reaction method of synthesis. An investigation was conducted to examine the porosity and bioactive properties of different CaO/SiO_2 ratios for potential use in bone reconstruction. The study identified that a material composition consisting of 40 wt.% CaO and 60 wt.% SiO_2, sintered at 800 °C for 1 h, exhibited optimal characteristics. In this composition, the formation of pseudo-wollastonite was observed, resulting in the lowest porosity and a high density of 2.6 g/cm^3. Furthermore, in the case of a composition comprising 50 wt.% CaO and 50 wt.% SiO_2, a transition from pseudo-wollastonite to wollastonite phase was detected. Elevated calcium content resulted in heightened apparent porosity, achieving a maximum purity of 19%. Furthermore, Yudha S.S. et al. described the synthesis of calcium silicate derivatives utilizing natural resources such as eggshell (ES) as a calcium source and oil palm leaves (OPL) for silica. Through a solid-state reaction, they successfully synthesized powder materials containing calcium silicate derivatives, primarily Ca_2SiO_4, with a minor presence of $CaSiO_3$. [112] The findings of their study indicate that the concentration of the precursors plays a significant role in influencing the surface morphology and crystallinity of the final powders, particularly in relation to the irregularities observed in the micrometer-sized particles. Gaurav Sharma et al. [113] prepared CS glass ceramic using agro-food waste via the melt-quenching method followed by heat treatment at 900 °C for 10 h. They mixed different wt.% of eggshells, rice husk, and sugarcane leave ash powders followed by sintering at 900 °C for 10 h. R. Reddappa et al. [114] studied the luminescence properties of Er^{3+} doped di-calcium silicate synthesized from eggshells and rice husks using a high-temperature solid-state technique. The decay curves of the emitting levels in the phosphors display a non-exponential nature across all concentrations. This behavior can be attributed to the dipole–dipole interaction occurring between the Er^{3+} ions. In the case of Ca_2SiO_4 phosphors, the lifetimes of the $^4S_{3/2}$ state of Er^{3+} ions were observed to decrease from 4 to 2.7 µs as the Er^{3+} content increased from 0.01 to 1.0 mol %. Further they synthesized Ln^{3+} doped Ca_2SiO_4 phosphors for solid state lighting [115]. J.P. Nayak et al. [116] also investigates the in-vitro bioactivity and biodegradability of calcium silicate material prepared using rice husk through a sol–gel route at 700 °C calcination temperature for 2 h holding time. Their findings revealed that the prepared material exhibited excellent

bioactivity, as evidenced by the formation of a carbonated hydroxyapatite phase during incubation. Hamisah Ismail et al. [117] reported the preparation of nano-wollastonite from rice husk ash and limestone using the sol–gel method. They investigate that the period of the calcination process must be controlled to get the appropriate grain size. They observed that with a holding time of 1 h, nano-size grains are obtained and by increasing the holding time to 2 h grain sizes over 100 nm were found. So, to get the desired size of grain we have to optimize the calcination temperature as well as the holding time. In their study, Rajan Choudhary et al. [118] synthesized a bioceramic material called calcium magnesium silicate using eggshells as a calcium source. The sol–gel method was employed for the synthesis process. To create the requisite initial solutions, solutions of 1 M magnesium nitrate and 3 M citric acid were produced using deionized water. During the synthesis process, quantities of 20 ml of eggshell solution, 20 ml of magnesium nitrate solution, and 30 ml of citric acid solution were individually drawn using pipettes from the previously prepared stock solutions. Subsequently, these distinct solutions were combined sequentially with 9 ml of tetraethyl orthosilicate (TEOS) within a beaker. The pH of the resulting reaction mixture was adjusted to 1 through the addition of concentrated nitric acid. Notably, nitric acid played a dual role within the sol–gel combustion methodology: it both maintained the pH of the reaction mixture at a value of 1 and facilitated the hydrolysis process of TEOS, leading to the formation of silanol and ethyl alcohol. The researchers discovered that when the sample was calcinated at 1200 °C for 6 h, the major phase observed was akermanite, with a minor phase of merwinite also present. Hossein Mohammadi et al. [119] prepared dense bulk calcium magnesium silicate using cockleshells (Ca source), rice husk (Si source), and dolomite as a magnesium source with a relative density of 93.50%. They used a high-energy planetary ball milling technique to mix cockleshells, rice husk, and dolomite in a 2:2:1 molar ratio to get a pure calcium magnesium silicate single phase. Shivani Punj et al. [120] used sustainable biomass wastes for the preparation of bioactive CS glass. Sugarcane, eggshells, and corn wastes are used as initial precursors for CS glass by applying the melt quenching technique at 1550 °C temperature. They found that the glasses derived from the bio-waste show better bioactivity than mineral-derived glasses due to the inherent porosity present in the bio-waste materials. Senthil Kumar Venkatraman et al. [121] prepared monticellite and diopside materials from eggshell waste using a combustion route. Diopside demonstrated phase purity at a temperature of 900 °C, while monticellite achieved phase purity at 1200 °C. Scanning electron microscopy (SEM) analysis revealed distinct morphological characteristics for each phase. Monticellite exhibited a beehive-like morphology, whereas diopside displayed porous rock-like structures. Naveen Subramaniam Vijayakumar et al. [122] reported the conversion of biowaste into larnite (β-di-calcium silicate) by the sol–gel method. They found a pure phase of larnite at 850 °C calcination temperature. So, there is huge literature available on the synthesis of calcium silicate and its derivatives by using food, agricultural, and industrial waste material. Table 2 shows the literature available for the combination of different silica and calcium bio-waste for various material synthesis.

5 Applications

5.1 Tissue Engineering

The biomedical applications of Calcium (Ca), silica (Si), and magnesium (Mg) ions have garnered considerable attention. These ions play crucial roles in various biological processes [123]. Calcium plays a crucial role in the regulation of cellular responses to bioceramics, as well as in facilitating cell growth and promoting the differentiation of cells into osteoblasts. In natural bone, calcium is present in the active region and holds significance in both blood vessels and bone growth [124]. Researchers indicates that by varying calcium concentrations there are having distinct effects: low concentrations (2–4 mmol) are conducive to the proliferation and differentiation of osteoblasts, medium concentrations (6–8 mmol) favor the development of the extracellular matrix, while higher concentrations (> 10 mmol) have been observed to be toxic to cells [125]. Extracellular calcium serves a crucial biological function in the regulation of bone restoration, operating independently of hormones through the activation of cation-sensing receptors. Furthermore, it has the capacity to enhance the effectiveness of insulin-like growth factor, a key regulator of osteoblast proliferation [126]. By stimulating cation-sensing receptors and facilitating the actions of insulin-like growth factors, extracellular calcium plays a significant role in promoting the growth and proliferation of osteoblasts [127]. Silica, however, plays a vital role in the process of bone calcification, contributing to the enhancement of bone density and the prevention of osteoporosis. Silicon (Si) has remarkable benefits for the structure and function of bone tissue and is closely linked to calcium in regulating bone metabolism [128]. The mounting evidence suggests that silicon (Si) exerts a positive influence on maintaining bone homeostasis. Si is typically absorbed in the form of metasilicate, which is widely distributed in connective tissue throughout the body. Importantly, Si has the capacity to stimulate bone formation, contributing to the overall health and strength of the skeletal system [129]. Stimulation with silicon (Si) in MG63 osteoblasts has demonstrated notable effects on cell proliferation and significantly enhanced the expression

Table 2 The literature available for the combination of different silica and calcium bio-waste for various material synthesis

Ref	Biowaste material								Yield Material	Method of synthesis and calcination temperature
	Egg shells	Snail shells	Rice husk	Coconut husk	Sugarcane bagasse	Peanut shells	Fly Ash	GGBS		
Rimruthai Phuttawong et al. [108]		✓	✓						Calcium silicate	Solid-state reaction method Temp.: 1000 °C
Sadang Husain et al. [172]		✓	✓						Calcium silicate	Solid-state reaction method Optimum Temp.: 900 °C to 1100 °C
Srinath Palakurthy et al. [173]	✓		✓						Calcium silicate	Sol–gel method Temp.: 900 °C
Pooja yadav et al. [174]							✓	✓	Akermanite	Sol–gel method Temp.: 950 °C
M. Krishnam Raju et al. [175]	✓		✓						Calcium silicate	Hydrothermal method Temp.: 135 °C for 24 h
Rajan Choudhary et al. [118]	✓		✓						Silicate ceramics: Wollastonite (W), Diopside (D) and Forsterite (F)	Solid-state reaction method Temp.: 1100 °C for W, 1250 °C for D and 1300 °C for F
Manmeet Kaur Chhina et al. [109]	✓		✓						Di-calcium silicate	Solid-state reaction method Temp.: 1250 °C
Ruby Priya et al. [176]	✓				✓				Di-calcium silicate	Solid-state reaction method Temp.: 900 °C
Shivani punj et al. [120]	✓				✓				Calcium silicate glass	Melt-quenching technique Temp.: 1550 °C
Hossein Mohammadi et al. [119]		✓	✓						Akermanite	High-energy planetary ball milling Temp.: 1250 °C
Srinath Palakurthy et al. [177]	✓		✓						Diopside	Sol–gel method Temp.: 800 °C
Gaurav Sharma et al. [113]	✓		✓		✓				Glass–ceramic	Melt-quenching technique Temp.: 900 °C
Satwinder Singh Danewalia et al. [178]			✓		✓				Cristobalite	Solid-state reaction method Temp.: 1000 °C
Nur Hazlinda Jakfar et al. [179]	✓		✓						Calcium mono silicates	Mechanochemical route Temp.: 1300 °C

of collagen type I genes. This enhancement is believed to be a result of the activation of the extracellular signal-regulated kinases (ERK) pathway. The induction of the ERK pathway is hypothesized to be responsible for the observed cellular responses in terms of increased cell growth and collagen synthesis in MG63 osteoblasts [130]. Promising biomaterials known as bioceramics, including β-tricalcium phosphate, wollastonite, diopside, akermanite, and others, exhibit exceptional properties that make them biologically compatible. These materials possess remarkable characteristics such as corrosion resistance, resistance to bacterial contamination, high compressive strength, and wear resistance [129, 131, 132]. Ceramics possess the advantage of being compatible with the internal environment of the body due to their specific chemical composition and their ability to dissolve into ionic components. This dissolution process facilitates the release of bioactive ions, such as Ca^{2+} and Mg^{2+}, which trigger beneficial biological reactions within the body. Simultaneously, ceramics also release low-toxicity ions like Al^{3+} and Zr^{4+}, which have minimal adverse effects on body tissues [133]. The biodegradability of magnesium (Mg) has garnered significant attention in the biomedical field [134]. It has emerged as a promising material due to its mechanical properties, resembling those of human bone (density of 1.74 g/cm^3 and elastic modulus of 41–45 GPa), and its excellent biocompatibility. In addition to its structural resemblance to bone, magnesium is also an essential nutrient for maintaining human health. Magnesium alloys play a supportive role in bone growth by promoting cell adhesion to biomaterials and facilitating the differentiation and biomineralization of osteoblasts. However, one characteristic worth noting is the susceptibility of magnesium alloys to corrosion in a physiological environment due to their active chemical nature. Consequently, they gradually degrade over time, resulting in the formation of magnesium hydroxide [$Mg(OH)_2$] and hydrogen (H_2). Importantly, the corrosion products of magnesium alloys have been extensively studied and proven to be non-toxic when compared to other metal implants. These corrosion byproducts can be safely eliminated from the body through the natural processes of human metabolism. [135]

Consequently, both CS and its derivatives possess the capacity to stimulate the formation of hydroxyapatite when immersed in simulated body fluid (SBF). There are various steps for the formation of a hydroxyapatite layer onto the CS when immersed in SBF as mentioned in Fig. 8. During the initial stage, an exchange occurs between calcium ions (Ca^{2+}) and hydrogen ions (H^+) in the simulated body fluid (SBF) solution, resulting in the release of Ca^{2+} ions. In this process, the dissolution of calcium (Ca) and silicon (Si) follows an incongruent pattern, where there is a higher preference for the release of Ca ions compared to Si ions [136]. Consequently, a leached layer forms, characterized by an abundance of silanol groups (≡Si–OH). In the subsequent phase, the Ca^{2+} ions present in the SBF solution are electrostatically attracted to the newly formed layer enriched with silanol groups, which carry a negative charge. As the Ca^{2+} ions accumulate on the surface, the pH of the leached solution rises due to the preferential dissolution of Ca^{2+} ions. This elevated pH level enhances the state of supersaturation in relation to apatite, facilitating the precipitation of apatite. In the third step, the Ca^{2+} ions adhere to the negatively

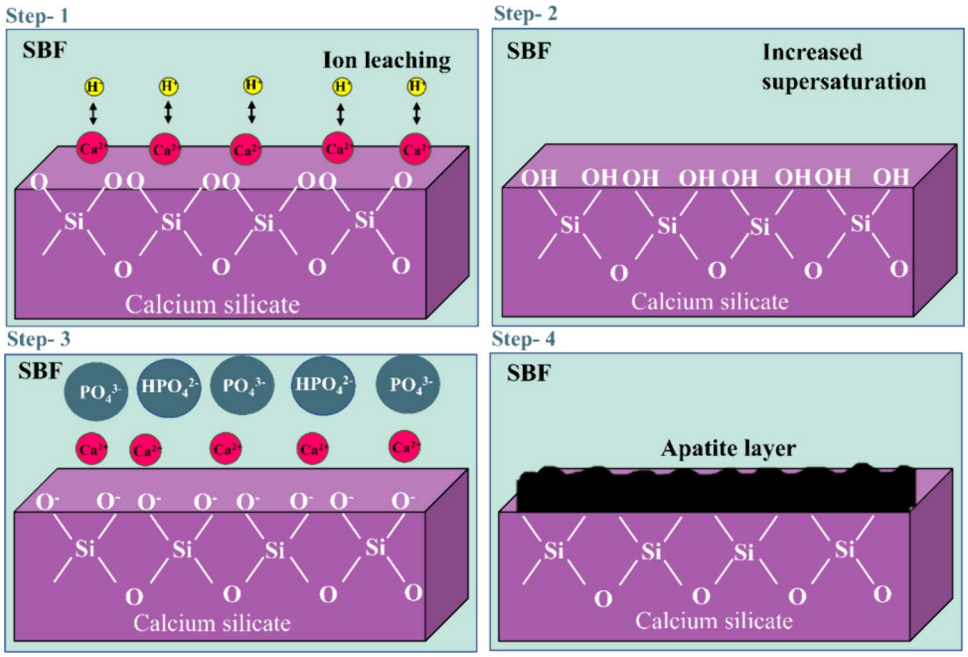

Fig. 8 Schematic of apatite layer formation on calcium silicate material after being kept in SBF solution

charged surface decorated with silanol groups (≡Si–OH), driven by electrostatic attraction. Subsequently, phosphate ions (PO_4^{3-}/HPO_4^{2-}) from the SBF solution adsorb onto the Ca^{2+} ions. This adsorption process leads to the formation of a layer composed of apatite with a bone-like composition on the surface of CaO-SiO_2-based ceramics. [137]

In a study conducted by Junying Sun et al. [138], revealed the positive impact of ionic products derived from a plasma-sprayed dicalcium silicate coating on the proliferation and differentiation of MG63 osteoblast-like cells. The dissolution products of the dicalcium silicate coating, in their ionic form, demonstrated the ability to promote cell mineralization and potentially enhance osteoblastic differentiation through autocrine BMP2 signaling. This research highlights the potential of utilizing dicalcium silicate coatings to facilitate favorable cellular responses and support the development of osteoblast-like cells. Miao Sun et al. [139] conducted a study to examine the biological effectiveness of a bone cement based on β-dicalcium silicate (β-C2S) in comparison to the widely used calcium phosphate cement (CPC) in clinical settings. The findings of their research clearly indicated that the β-C2S composite exhibited superior characteristics, including accelerated degradation, increased release of calcium ions (Ca^{2+}) and silicon ions (Si^{4+}), as well as the ability to stimulate cell proliferation and enhance alkaline phosphatase activity during in vitro experiments.

Based on their findings, the researchers reached the conclusion that the β-C2S-based cement exhibits tremendous potential as a bone implant for the purpose of bone regeneration and repair. This conclusion is supported by the remarkable biological performance demonstrated by the cement, both in laboratory settings (in vitro) and within living organisms (in vivo). In their research, Siriphannon et al. [140] made an intriguing discovery regarding the surface of pure $CaSiO_3$ ceramic. The researchers noted that the synthesized ceramic demonstrated a faster rate of hydroxyapatite (HA) formation compared to other biocompatible materials like apatite wollastonite A/W glass–ceramics and various bioactive glass–ceramics. Through in vitro cell culture assessments, it was observed that the wollastonite ceramics exhibited the ability to facilitate the adherence of osteoblast-like cells and bone marrow mesenchymal stem cells. Furthermore, these ceramics displayed the potential to enhance both cell proliferation and differentiation. In addition to their biological properties, wollastonite ceramics showcased improved mechanical characteristics, including higher fracture toughness and bending strength, when compared to calcium phosphate ceramics. In a study conducted by Weichang Xue et al. [141], a wollastonite coating was prepared using the plasma spraying method. The researchers aimed to investigate the bioactivity of this coating in vivo by implanting it in different locations within a dog's body, such as muscle, cortical bone, and marrow. The findings revealed that when implanted in the dog's muscles, the wollastonite coating led to the formation of a bone-like apatite layer on its surface. Similarly, when implanted in cortical bone, the wollastonite coating promoted the extension and growth of bone tissue while inhibiting the formation of fibrous tissue. These results demonstrate the promising bioactivity of the wollastonite coating, suggesting its potential application in facilitating bone regeneration and repair in vivo. A study conducted by Songfeng Xu et al. [142] aimed to assess the in vivo bone-regenerative properties and resorption characteristics of porous β-calcium silicate (β-CaSiO3, β-CS) bioactive ceramics. The investigation utilized a rabbit calvarial defect model and compared the obtained results with porous β-tricalcium phosphate (β-Ca3(PO4)2, β-TCP) bioceramics. Through quantitative analysis, the researchers discovered that β-CS showcased a notably faster resorption rate and demonstrated superior capabilities for bone regeneration in vivo when compared to β-TCP. In their research, Zhiyun Du et al. [143] developed a scaffold made of calcium silicate (CS) and incorporated doping elements such as Mg^{2+} or Mn^{2+}. This was done because the physicochemical properties of bone tissue engineering (BTE) scaffolds, including their chemical composition, morphology, microarchitecture, degradation, and stiffness, significantly influence cell activities. The incorporation of Mg^{2+} or Mn^{2+} into the CS scaffold further enhances its ability to promote osteogenesis (bone formation) and angiogenesis (blood vessel growth). In their study, Shao et al. [144] conducted a systematic evaluation of the influence of side-wall pore architecture on the mechanical properties and osteogenic capacity of direct-ink-written bioceramic scaffolds. They specifically focused on rabbit calvarial defects and fabricated calcium silicate scaffolds doped with magnesium (Mg) at varying layer thicknesses and macropore sizes. The findings highlighted the significance of side-wall pore architecture in 3D-printed bioceramic scaffolds for optimal bone repair in calvarial bone defects. Additionally, the study demonstrated the promising potential of Mg-doped wollastonite for 3D printing thin-wall porous scaffolds in the treatment of craniomaxillofacial bone defects, surpassing the capabilities of pure calcium silicate scaffolds.

Derived from calcium silicate, calcium magnesium silicate ceramics demonstrate enhanced mechanical strength and a reduced dissolution rate in comparison to wollastonite ceramics. This improvement can be attributed to the higher energy of the Mg-O bond relative to the Ca-O bond within the crystal structure. The heightened bond energy contributes to the stability of the crystal system, leading to a slower dissolution rate. Consequently, the mechanical properties of calcium magnesium silicate ceramics are enhanced due to the restricted rapid dissolution rate and the overall improved stability of the crystal structure. Chengtie Wu et al. [145] successfully fabricated akermanite ceramic

through a sintering process conducted at a temperature of 1370 °C for 6 h. The primary focus of the study was to evaluate the mechanical properties of the resulting material. The research revealed that the akermanite ceramics demonstrated a noteworthy bending strength of 176 MPa. Additionally, the fracture toughness was measured at 1.83 $MPam^{1/2}$. Moreover, when subjected to immersion in simulated body fluid (SBF), the akermanite ceramics displayed the capability to induce the formation of hydroxyapatite (HAp) on their surface. Notably, akermanite exhibited superior osteogenesis and biodegradation properties compared to β-tricalcium phosphate. At later stages of implantation, the rate of bone formation was observed to be faster in akermanite than in β-tricalcium phosphate [146]. Previous research indicated that diopside ceramics exhibited a bending strength of 300 MPa, a fracture toughness of 3.5 $MPam^{1/2}$, and a Young's modulus of 170 GPa. Comparatively, the bending strength and fracture toughness of akermanite ceramics were found to be lower than those of diopside ceramics, while the Young's modulus of akermanite ceramics closely resembled that of cortical bone, unlike diopside ceramics. In more specific terms, diopside scaffolds demonstrated an initial compressive strength ranging from 0.63 to 1.36 MPa, along with porosities ranging from 75 to 80%. These values are similar to the compressive strength observed in cancellous bone. These characteristics underscore the significant potential of diopside in bone implant applications that require slow dissolution or enhanced chemical stability. [147]

In recent years, researchers have directed their attention towards the recycling of natural waste as an alternative means of producing CS. Vichaphund and colleagues [148] achieved the successful synthesis of wollastonite using a solid-state reaction assisted by microwave irradiation. They employed a combination of eggshell and silica as the raw materials for the synthesis process. Anjaneyulu and Sasikumar [149] showcased the advantageous bioactivity of nanocrystalline wollastonite. This specific form of wollastonite was synthesized utilizing eggshell as a calcium source through the sol–gel combustion method. Abd Rashid R et al. [150] presented a comprehensive outline of the bioactive attributes exhibited by wollastonite originating from Malaysian limestone and silica sand. Upon immersion in simulated body fluid (SBF), they noted the formation of a calcium-deficient hydroxyapatite layer on the surface of the synthesized wollastonite. Saravanan S et al. [151] investigation revolved around employing rice straw ash as a silica source to synthesize wollastonite, culminating in the creation of a mesoporous structure. Their study showcased that the generated wollastonite particles exhibited osteoconductive qualities, fostering the proliferation of mouse mesenchymal stem cells and orchestrating cyclin expression across different phases of the cell cycle. In our research group, we have successfully devised a technique to produce wollastonite, utilizing rice husk for its silica content and eggshell as a calcium oxide source. Our adapted sol–gel methodologies enabled us to attain markedly lower sintering temperatures. The resultant synthesized wollastonite displayed remarkable in vitro bioactivity, manifesting a diminished degradation pace and negligible pH fluctuations within physiological fluids when compared to wollastonite prepared using $Ca(NO_3)_2.4H_2O$ and TEOS. Moreover, this synthesized wollastonite showcased potential antimicrobial attributes, exceptional compatibility with MG-63 cells, and a substantial stimulation of cell growth.

5.2 Drug Delivery

Multiple factors must be taken into account for drug delivery applications: (i) Biocompatibility: The delivery system must be non-toxic, non-immunogenic, and should not trigger adverse reactions within the body. (ii) Targeting Capability: The system should have the ability to precisely deliver the drug to a specific site of action, such as a tumor or a particular organ. (iii) Controlled Release: The delivery system should enable controlled and sustained release of the drug, ensuring the desired rate and duration of action. (iv) Stability: The system should exhibit stability under storage conditions and in the presence of body fluids to maintain the integrity and effectiveness of the drug. (v) Scalability: The delivery system should be easily scalable to accommodate the requirements of mass production, allowing for efficient and large-scale manufacturing [152, 153]. CS exhibits great potential as a material for drug delivery vehicles in targeted drug delivery applications. This is attributed to its exceptional biocompatibility, bioactivity, biodegradability, high drug loading capacity, and pH-responsive drug release properties. CS is known for its biocompatible nature, ensuring that it does not provoke any adverse reactions upon introduction to the body. [3]

The inclusion of calcium as a constituent in biocompatible materials is of significant importance. The introduction of calcium can enhance the properties of materials, such as increasing their biocompatibility, high drug loading capacity, and facilitating long-term drug release. In CS carriers, the presence of Ca^{2+} ions allow for interactions with functional groups found in drug molecules that contain carboxyl (-COOH) and hydroxyl (-OH) groups, such as ibuprofen, aspirin, and amoxicillin. As a result, calcium silicate-based carriers often exhibit remarkably high drug loading capacities [154]. Moreover, calcium silicate (CS) material serves multiple purposes in cosmetic formulations, such as functioning as an absorbent, bulking agent, and opacifying agent. In the year 1998, the U.S. Food and Drug Administration (FDA) recorded a total of 132 formulations that incorporated calcium silicate, and among these formulations, face powders constituted approximately 30%. Additionally, calcium

silicate (CS) finds its place in the OTC Active Ingredient Status Report as both an external analgesic and a skin protectant. This classification underscores the recognized utility of CS in topical applications [155]. Jin Wu et al. [156] introduced an economical and surfactant-free approach for accomplishing the sono-chemical synthesis of hierarchically nanostructured mesoporous microspheres composed of calcium silicate hydrate (CSH). These microspheres, formed from nanosheets and denoted as HNMS-CSH, were achieved without relying on traditional surfactant templates. Typically, surfactants play a role as templates in generating mesoporous architectures and porous surfaces embedded with organic groups, facilitating drug adsorption and controlled release. Nonetheless, the persistence of residual surfactants and introduced organic components could potentially induce cytotoxicity, thus curtailing their viability in clinical applications. The prepared nanosheets exhibited a thickness of approximately 30 nm, a diameter of around 1 μm, a pore size of 10.8 nm, a surface area of 290 m^2g^{-1}, and a pore volume of 1.20 cm^3g^{-1}. Remarkably, the ibuprofen drug loading capacity was found to be exceptionally high at 2.29 g of ibuprofen per gram of carrier. This can be attributed to the ultrahigh specific surface area of the HNMS-CSH and the strong interaction between ibuprofen and the drug carrier. Ibuprofen molecules ($((CH_3)_2CHCH_2PhCH(CH_3)COOH$) were capable of forming linkages with HNMS-CSH nanosheets through electrostatic bonding between the Ca^{2+} cation of the carrier and the COOH group of ibuprofen molecules. The study demonstrated that the drug release system exhibited a slow and sustained release of ibuprofen, lasting for over 500 h. The researchers also introduced a novel drug release kinetics model for the calcium silicate hydrate drug delivery system. This model established a linear relationship between the cumulative amount of released drug (C) and the natural logarithm of the release time (t), represented by the equation: $C = k \cdot \ln(t)$, where k represents a constant. A schematic depicting the drug loading and drug release processes can be found in Fig. 9.

Meili Zhang et al. [157] employed a surface-assisted sonochemical method to prepare hollow calcium silicate hydrate (CSH) microspheres with a diameter of approximately 1 μm. Surfactants were utilized in the microsphere preparation process as ultrasound radiation can induce the formation of surfactant vesicles, which serve as templates for achieving the desired sphere morphology. BET analysis revealed that the specific surface area of the hollow CSH sphere was 137.5 m^2/g, significantly higher than the 16.2 m^2/g observed for conventional CSH powders. Consequently, the amount of gentamicin loaded onto the CSH hollow spheres was 26.2 ± 1.6 wt% (~260 mg/g), which was approximately 13 times greater than that loaded onto conventional CSH powders (2.1 ± 0.2 wt%, equivalent to ~20 mg/g). This substantial difference in drug loading capacity can be attributed to the higher specific surface area of the hollow CSH spheres compared to the powdered form. Notably, the release of gentamicin from the hollow CSH spheres after 72 h was only 30 wt%, significantly lower than the 60 wt% observed for conventional CSH powder. This configuration minimizes the risk of sudden bursts or rapid release of drugs upon immersion in a solution. Duo Wang and colleagues prepared europium-doped mesoporous calcium silicate (MCS) nanoparticles with sizes ranging from 60–110 nm through a hydrothermal synthesis route. BET analysis demonstrated a pore size of 2.98 nm, a specific surface area of 310.85 m^2/g, and a pore volume of 0.67 cm^3/g for the prepared material. Europium-doped mesoporous calcium silicate exhibited a remarkable capacity to accommodate a high quantity of the anticancer drug anthracycline doxorubicin, indicating its exceptional drug-loading capability. The study further revealed that only 5.92% of the doxorubicin was released at pH 7.4, while nearly 20% was released in an acidic medium at pH 5.0, highlighting its pH-responsive drug release behavior. The drug-loaded Eu-calcium silicate displayed low cytotoxicity, pH-controlled drug release properties, and emitted intense red light at 613 nm upon UV irradiation. The luminescence behavior of the material is particularly advantageous for drug delivery applications as it enables easy detection through biological tissue without causing damage. Xue et al. [103] conducted a research endeavor in which they employed a wet chemical approach to prepare mesoporous calcium silicate. They subsequently induced the creation of mesopores within the material through an acid-based modification using hydrochloric acid. This acid-induced alteration led to the development of a hydrated silica gel layer on the surface of the calcium silicate, enriched with functional Si–OH groups. This surface layer showcased a mesoporous

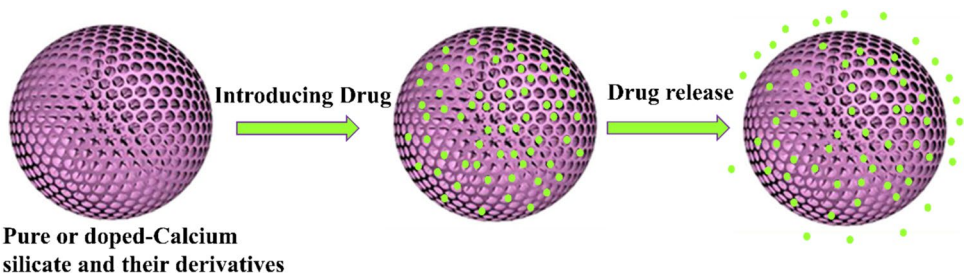

Fig. 9 The figure presents a schematic depiction of the experimental procedure for drug loading and drug release loaded in pure or doped-calcium silicate and their derivatives

arrangement featuring pore diameters spanning from 4 to 5 nm. The mesoporous calcium silicate exhibited varying BET-specific surface areas contingent upon the pH conditions. Specifically, surface areas of 221, 333, and 356 m^2g^{-1} were achieved at pH levels of 7, 4.5, and 0.5, respectively. In stark contrast, the unmodified calcium silicate material displayed a surface area of only 65 m^2g^{-1}. Furthermore, the mesoporous calcium silicate displayed markedly enhanced loading capabilities for bovine serum albumin and lysozyme in comparison to the unmodified material. The release kinetics of proteins from the mesoporous calcium silicate demonstrated a sustained release profile over a span of one week, while proteins loaded onto the unmodified material exhibited rapid burst release kinetics within a few hours. In their study, Fan et al. [158] innovated a luminescent and mesoporous mechanism for drug delivery by crafting europium-doped calcium silicate. This design presented a remarkable loading capacity, accommodating 21 wt% of ibuprofen, with drug release spanning 12 h. Under exposure to UV light, the system emitted a distinctive red luminescence, attributed to Eu^{3+}. Notably, an intriguing discovery emerged: even subsequent to the drug loading, the emission intensities of Eu^{3+} within the drug delivery system fluctuated in tandem with the quantity of ibuprofen released. This remarkable observation implies that the course of drug release could be effectively traced and observed by monitoring alterations in the luminescence intensity of the drug delivery system. Using mesoporous silica spheres as templates, Kang et al. [159] created luminescent and mesoporous microspheres doped with Eu^{3+} and Tb^{3+} in the calcium silicate matrix. When excited by UV light, the microspheres loaded with around 20 wt% of ibuprofen exhibited distinct emissions from both Eu^{3+} and Tb^{3+} ions. Interestingly, the photoluminescence intensity of Eu^{3+} ions within the drug delivery system exhibited a direct correlation with the cumulative amount of released ibuprofen. This noteworthy finding implies that the luminescence intensity could serve as a valuable indicator for real-time monitoring of the drug delivery process.

5.3 Optoelectronic

Over the past ten years, there has been extensive research on rare-earth (RE)-activated nano phosphors, primarily due to their applications in lighting. These advanced materials have swiftly replaced traditional lighting technologies like incandescent bulbs, owing to their remarkable benefits [160]. Nano phosphor-based light-emitting diodes (LEDs) have proven to be environmentally friendly, exceptionally reliable, and energy-efficient, which has led to their rapid adoption. One of the key reasons for this notable shift is the eco-friendliness of these LEDs. They offer significant advantages such as reduced energy consumption and an extended lifespan [161]. Furthermore, their use of inorganic nano phosphors has effectively addressed the demand for lighting solutions that operate with low-input voltage. This combination of features has propelled the widespread acceptance and implementation of these LEDs.

The outstanding characteristics of CS make them widely recognized as the optimal host materials for luminescence centers. These materials exhibit exceptional chemical and thermal stability, ensuring their durability in various environments [162]. CS also boast a long persistence time, enhancing their ability to emit light. Their superior formability allows for the creation of intricate structures, further expanding their applications. Silicates are known for their capacity to generate multicolor phosphorescence, adding versatility to their utility [163]. Additionally, they can be easily prepared, simplifying their incorporation into different systems. One of the key benefits of using calcium silicate is that it has high chemical stability and is resistant to corrosion. This makes it an excellent choice for use in harsh environments where other materials may degrade or break down. Another important property of calcium silicate is that it has a relatively low phonon energy, which means that it can efficiently transfer energy to luminescent centers embedded within the lattice. This property is important because it allows for efficient energy transfer, which leads to brighter and more efficient luminescence [164]. Moreover, calcium silicate possesses a broad bandgap, making it suitable for the development of luminescent materials that emit light within the visible or near-infrared spectrum. Additionally, its high thermal conductivity enables efficient dissipation of heat. Researchers have shown significant interest in the utilization of rare earth or transition metal ions doped silicates due to their remarkable luminescence emission in the blue, green, and red regions of the electromagnetic spectrum. [158]

Hyun-Joo Woo et al. [165] conducted research on the development of Eu^{2+}:Ca_2SiO_4 phosphor using propylene glycol modified silane (PGMS) with different aging periods. They employed a novel sol–gel technique to achieve tunable emission from a single host by utilizing PGMS as a silicate source. By incorporating differently aged PGMS into $Ca_{1.95}Eu_{0.05}SiO_4$ phosphors, they successfully adjusted the luminescence characteristics from reddish yellow to green. This study offers valuable insights into creating a tunable luminescence system by controlling the α, β, and γ crystal phases of Ca_2SiO_4 through the use of differently aged silicate sources. Moreover, the findings provide practical knowledge for developing color-tunable LED-based light sources capable of generating diverse lighting environments using a single host material. In a related work, Hyun-Joo Woo et al. fabricated calcium silicate phosphors (Ca_2SiO_4:Eu^{3+}) activated with Europium ions via the hydrothermal method. They controlled the size of the prepared phosphor particles, resulting in sharp red-light emission. The researchers achieved a high photoluminescence quantum yield of over 87.95% and

obtained exceptional color purity of 99.8%. They explained that the intensity of the $^5D_0 \rightarrow {}^7F_4$ emission transition in Eu^{3+} was influenced by structural distortion caused by reductions in particle size. Yoshiyuki Kojima et al. [166] synthesized a red-emitting phosphor material composed of amorphous calcium silicate activated by Eu^{3+}. Their study focused on the significant impact of water removal from the interlayers of the calcium silicate hydrate (CSH) phosphor on the emission intensity. The researchers observed a remarkable increase in emission intensity upon removing the OH group, which is present as a water molecule within the host structure. M.S. Upendra Rao et al. [167] conducted a study to investigate the influence of charge compensation on the photoluminescence characteristics of silicates. They utilized alkali metals (Li^+, Na^+, K^+) and other halogens (Cl^-) as charge compensators in their research. Specifically, they focused on an alkali metal pair, where the charges are identical but the size and mass ratios differ significantly. To prepare their samples, the researchers employed europium-doped calcium silicate (Ca_2SiO_4: Eu^{3+}) with various charge compensators, including alkali metals such as Li, Rb, and a combination of Li-Rb. Hsien-Wei Tseng et al. [168] undertook a research investigation into the photoluminescence properties of Eu-doped $Ca_2MgSi_2O_7$ phosphors. They prepared these phosphors under different atmospheric conditions and denoted them as $Ca_{2+x}MgSi_2Eu_{0.025}O_{7+x}$, with x representing a varying parameter. When prepared under normal air atmosphere, these phosphors emitted a red color. However, when prepared under a reduction atmosphere, they exhibited the highest intensities for both photoluminescence excitation (PLE) and photoluminescence (PL). The intensity of both PLE and PL increased with higher x values, indicating a direct correlation between the dopant concentration and emission intensity. Furthermore, the emitted light color varied with different x values. For x values of 0 and 0.2, the emitted light appeared green. As x increased to 0.4, the color changed to cyan, followed by cyan-blue for $x = 0.6$, and finally blue for x values of 0.8 and 1.0. In another related study conducted by Sahu et al., they explored a Ce^{3+}-doped $Ca_2MgSi_2O_7$ phosphor. Upon excitation at a wavelength of 327 nm, the phosphor exhibited two distinct emission bands. These bands had central wavelengths of 373 nm and 393 nm, resulting in a broadband peak at 385 nm. Sahu et al. [169] employed Eu^{2+} and Dy^{3+} as co-doped ions in the $Ca_2MgSi_2O_7$ phosphor. The synthesized phosphor emitted green light, with a central wavelength of 535 nm. In a separate study by Cao et al. [170], they utilized Eu^{2+} and Tm^{3+} as co-doped ions in the $Ca_2MgSi_2O_7$ phosphor. They observed that with an increase in the synthesis temperature from 1250 to 1350 °C, the central emission wavelengths underwent a shift from 475 to 521 nm. Interestingly, the Eu^{2+}-doped $Ca_2MgSi_2O_7$ phosphor, as well as most of the Eu^{2+}-based multi-ion doped $Ca_2MgSi_2O_7$ phosphors, emitted green light. Furthermore, phosphors based on $Ca_3MgSi_2O_8$ have attracted significant attention from researchers due to their high quantum efficiencies (η) and thermal stability, leading to prolonged and intense interest in their exploration. Dewangan et al. [171] examined the luminescence characteristics of a Dy^{3+} doped $Ca_3MgSi_2O_8$ phosphor excited at a wavelength of 351 nm. The emission spectrum of the phosphor displayed three distinct peaks, positioned at 482 nm, 493 nm, and 574 nm, representing blue and yellow light emissions. However, it is worth noting that $Ca_3MgSi_2O_8$ is typically doped either solely with Eu^{2+} ions or co-doped with Eu^{2+} ions along with other ions. In these cases, the emission peak predominantly occurs at around 480 nm, emitting either blue light or greenish-blue light.

6 Overview and Future Directions

This analysis discusses the large amount of waste that we produce from a variety of sources, including plants, industries, and food. This waste can harm the environment and people if we don't handle it properly. It might even cause diseases. About 80% of the crop leftovers in farming are wasted after being harvested. Normally, we burn this leftover material, which releases harmful air pollutants and greenhouse gases. This damages our health and raises Earth's temperature. The creation of nanomaterials like calcium silicate, diopside, akermanite, and other materials based on calcium and silica is a better way to use waste, though. These nanomaterials may prove to be very beneficial and reduce our energy consumption. This method of recycling waste is advantageous because it can be applied repeatedly and is reasonably priced. This study also explains how the waste impurities can enhance the optical, mechanical, and porosity properties of these nanomaterials.

A significant challenge still in this field due to the problem of waste's makeup is different in different parts of the world. This makes producing these nanomaterials on a large scale consistently difficult. To better understand how various waste types decay, more research is required. In this manner, we can gather the appropriate waste at the appropriate time to produce these nanomaterials. Additionally, since researchers have only so far attempted to synthesize materials, we need to figure out the material from the point of view of applications. Utilizing these waste-based materials in wearable technology is an additional intriguing concept. This has a lot of potential but needs more research. Being more environmentally friendly and avoiding the use of hazardous chemicals is possible by creating these nanomaterials from waste. Making nanomaterials from waste seems like a smart idea with many applications because we produce a lot of waste and it contains useful materials.

7 Conclusion

In conclusion, this succinct review explores recent advances made over a decade's time in the production of calcium silicate derivatives, which have a variety of applications in the medical field, including drug delivery, luminescence, gas sensor, and water treatment. According to a study covering the last two decades, the production of nanomaterials aided by biowaste has increased exponentially because of its accessibility, superior stability, and large surface area. In the end, it is found that using biowaste has more advantages than using other raw materials. These advantages include zero contamination, simple processes, low toxicity, high stability, and cost-effectiveness in the synthesis of new materials. With the right policy development from the government or other relevant authority, biowaste-assisted nano-synthesis could potentially be scaled up to meet sustainable green applications that open up new horizons and better tomorrow.

Author Contributions A:Write the manuscript B: Prepared the draft, reviewed the manuscript, concept C: prepare the figures, Tables D: Review the literature E: Review the literature

Funding The author thanks the MHRD, Government of India for providing financial support.

Data Availability No datasets were generated or analysed during the current study.

Declarations

Ethics Approval The manuscript has not been published.

Consent to Participate and Publication The authors consent to participate and publication.

Competing Interests The authors declare no competing interests.

References

1. Cavillon M, Dragic P, Kucera C, Hawkins TW, Ballato J (2019) Calcium silicate and fluorosilicate optical fibers for high energy laser applications. Opt Mater Express 9(5):2147. https://doi.org/10.1364/OME.9.002147
2. Youness RA, Tag El-deen DM, Taha MA (2023) A review on calcium silicate ceramics: properties, limitations, and solutions for their use in biomedical applications. SILICON 15(6):2493–2505. https://doi.org/10.1007/s12633-022-02207-3
3. Zhu Y-J, Guo X-X, Sham T-K (2017) Calcium silicate-based drug delivery systems. Expert Opin Drug Deliv 14(2):215–228. https://doi.org/10.1080/17425247.2016.1214566
4. Liu Z, He X, Chen S, Yu H (2023) Advances in the use of calcium silicate-based materials in bone tissue engineering. Ceram Int 49(11):19355–19363. https://doi.org/10.1016/j.ceramint.2023.03.063
5. Wu C, Chang J, Fan W (2012) Bioactive mesoporous calcium-silicate nanoparticles with excellent mineralization ability, osteostimulation, drug-delivery and antibacterial properties for filling apex roots of teeth. J Mater Chem 22(33):16801. https://doi.org/10.1039/c2jm33387b
6. Mitchell MJ, Billingsley MM, Haley RM, Wechsler ME, Peppas NA, Langer R (2021) Engineering precision nanoparticles for drug delivery. Nat Rev Drug Discov 20(2):101–124. https://doi.org/10.1038/s41573-020-0090-8
7. Shi J, Kuwahara Y, An T, Yamashita H (2017) The Fabrication of TiO2 supported on slag-made calcium silicate as low-cost photocatalyst with high adsorption ability for the degradation of dye pollutants in water. catal today 281:21–28. https://doi.org/10.1016/j.cattod.2016.03.039
8. Zhakiyeva Z, Cuello GJ, Fischer HE, Bowron DT, Dejoie C, Magnin V, Campillo S, Bureau S, Poulain A, Besselink R, Gaboreau S, Grangeon S, Claret F, Bourg IC, Van Driessche AES, Fernandez-Martinez A (2022) Structure of water adsorbed on nanocrystalline calcium silicate hydrate determined from neutron scattering and molecular dynamics simulations. J Phys Chem C 126(30):12820–12835. https://doi.org/10.1021/acs.jpcc.2c02626
9. Cho YJ, Kwon YJ, Jin S, Choi H, Lee J-H, Yang S-M, Choi S-W, Jeong YK (2022) Two-dimensional calcium silicate nanosheets for trapping atmospheric water molecules in humidity-immune gas sensors. J Hazard Mater 432:128671. https://doi.org/10.1016/j.jhazmat.2022.128671
10. Wu J, Zhu Y-J, Chen F (2013) Ultrathin calcium silicate hydrate nanosheets with large specific surface areas: synthesis, crystallization, layered self-assembly and applications as excellent adsorbents for drug, protein, and metal ions. Small 9(17):2911–2925. https://doi.org/10.1002/smll.201300097
11. Fernández-Rodríguez L, Durán A, Pascual MJ (2021) Silicate-based persistent phosphors. Open Ceram 7(January):100150. https://doi.org/10.1016/j.oceram.2021.100150
12. Gedeike I, Baltakys K, Eisinas A (2022) Thermal stability of synthetic high basicity calcium silicate hydrates substituted with Cr3+ ions. Mater Charact 193:112231. https://doi.org/10.1016/j.matchar.2022.112231
13. Venkataravanappa M, Basavaraj RB, Darshan GP, Daruka Prasad B, Sharma SC, Hema Prabha P, Ramani S, Nagabhushana H (2018) Multifunctional dy (III) doped di-calcium silicate array for boosting display and forensic applications. J Rare Earths 36(7):690–702. https://doi.org/10.1016/J.JRE.2017.11.013
14. Jayathilakan K, Sultana K, Radhakrishna K, Bawa AS (2012) Utilization of byproducts and waste materials from meat, poultry and fish processing industries: a review. J Food Sci Technol 49(3):278–293. https://doi.org/10.1007/s13197-011-0290-7
15. Abdel-Shafy HI, Mansour MSM (2018) Solid waste issue: sources, composition, disposal, recycling, and valorization. Egypt J Pet 27(4):1275–1290. https://doi.org/10.1016/j.ejpe.2018.07.003
16. Huaiwei Z, Xin H (2011) An overview for the utilization of wastes from stainless steel industries. Resour Conserv Recycl 55(8):745–754. https://doi.org/10.1016/j.resconrec.2011.03.005
17. Heriyanto, Pahlevani F, Sahajwalla V (2018) Synthesis of calcium silicate from selective thermal transformation of waste glass and waste shell. J Clean Prod 172:3019–3027. https://doi.org/10.1016/j.jclepro.2017.11.109
18. Hamad HN, Idrus S (2022) Recent developments in the application of bio-waste-derived adsorbents for the removal of methylene blue from wastewater: a review. Polymers (Basel) 14(4):783. https://doi.org/10.3390/polym14040783
19. Yadav P, Rao RP, Azeem PA (2023) Optical and structural properties of cost-effective nanostructured calcium titanate blue phosphor. Ceram Int 49(4):6314–6323. https://doi.org/10.1016/j.ceramint.2022.10.154

20. Chhina MK, Singh K (2020) Dy3+ and inherent Ti4+ activated Ca2SiO4 near white light emitting phosphors synthesized from agro-food waste ashes. Ceram Int 46(7):9370–9379. https://doi.org/10.1016/j.ceramint.2019.12.195
21. Owuamanam S, Cree D (2020) Progress of bio-calcium carbonate waste eggshell and seashell fillers in polymer composites: a review. J Compos Sci 4(2):70. https://doi.org/10.3390/jcs4020070
22. Falk G, Shinhe GP, Teixeira LB, Moraes EG, de Oliveira APN (2019) Synthesis of silica nanoparticles from sugarcane bagasse ash and nano-silicon via magnesiothermic reactions. Ceram Int 45(17):21618–21624. https://doi.org/10.1016/j.ceramint.2019.07.157
23. Bhagat SR, Mahajan L (2020) thermal power plant waste by-product and its utility in concrete. IOP Conf Ser Mater Sci Eng 970(1):012010. https://doi.org/10.1088/1757-899X/970/1/012010
24. Rastogi A, Kumar Paul V (2020) A critical review of the potential for fly ash utilisation in construction-specific applications in India. Environ Res Eng Manag 76(2):65–75. https://doi.org/10.5755/j01.erem.76.2.25166
25. Nguyen H-HT, Nguyen HT, Ahmed SF, Rajamohan N, Yusuf M, Sharma A, Arunkumar P, Deepanraj B, Tran H-T, Al-Gheethi A, Vo D-VN (2023) Emerging waste-to-wealth applications of fly ash for environmental remediation: a review. Environ Res 227:115800. https://doi.org/10.1016/j.envres.2023.115800
26. Alterary SS, Marei NH (2021) Fly ash properties, characterization, and applications: a review. J King Saud Univ - Sci 33(6):101536. https://doi.org/10.1016/j.jksus.2021.101536
27. Siddique R, Bennacer R (2012) Use of iron and steel Industry By-Product (GGBS) in cement paste and mortar. Resour Conserv Recycl 69:29–34. https://doi.org/10.1016/j.resconrec.2012.09.002
28. Okoro W, Oyebisi S (2023) Mechanical and durability assessments of steel slag-seashell powder-based geopolymer concrete. Heliyon 9(2):e13188. https://doi.org/10.1016/j.heliyon.2023.e13188
29. Ayilara M, Olanrewaju O, Babalola O, Odeyemi O (2020) Waste management through composting: challenges and potentials. Sustainability 12(11):4456. https://doi.org/10.3390/su12114456
30. Siddika A, Mamun MAAl, Alyousef R, Mohammadhosseini H (2021) State-of-the-art-review on rice husk ash: a supplementary cementitious material in concrete. J King Saud Univ - Eng Sci 33(5):294–307. https://doi.org/10.1016/j.jksues.2020.10.006
31. Bhuvaneshwari S, Hettiarachchi H, Meegoda J (2019) Crop residue burning in India: policy challenges and potential solutions. Int J Environ Res Public Health 16(5):832. https://doi.org/10.3390/ijerph16050832
32. Mignardi S, Archilletti L, Medeghini L, De Vito C (2020) Valorization of eggshell biowaste for sustainable environmental remediation. Sci Rep 10(1):2436. https://doi.org/10.1038/s41598-020-59324-5
33. Banerjee A, Panda S, Sidhantha M, Chakrabarti S, Chaudhuri B, Bhattacharjee S (2010) Utilisation of eggshell membrane as an adsorbent for carbon dioxide. Int J Glob Warm 2(3):252. https://doi.org/10.1504/IJGW.2010.036136
34. Waheed M, Yousaf M, Shehzad A, Inam-Ur-Raheem M, Khan MKI, Khan MR, Ahmad N, Abdullah, Aadil RM (2020) Channelling eggshell waste to valuable and utilizable products: a comprehensive review. Trends Food Sci Technol 106:78–90. https://doi.org/10.1016/J.TIFS.2020.10.009
35. Wani AK, Rahayu F, Fauziah L, Suhara C (2023) Advances in safe processing of sugarcane and bagasse for the generation of biofuels and bioactive compounds. J Agric Food Res 12:100549. https://doi.org/10.1016/j.jafr.2023.100549
36. Xu Q, Ji T, Gao S-J, Yang Z, Wu N (2018) Characteristics and applications of sugar cane bagasse ash waste in cementitious materials. Materials (Basel) 12(1):39. https://doi.org/10.3390/ma12010039
37. Li Y, Chai J, Wang R, Zhang X, Si Z (2022) Utilization of Sugarcane Bagasse Ash (SCBA) in construction technology: a state-of-the-art review. J Build Eng 56:104774. https://doi.org/10.1016/j.jobe.2022.104774
38. Prabhu N, Gajendran T, Karthikadevi S, Archana A, Arthe R (2021) Utilization of sugarcane bagasse for enhancement production of fibrinolytic enzyme using statistical approach. Clean Eng Technol 5:100269. https://doi.org/10.1016/j.clet.2021.100269
39. Kappil SR, Aneja R, Rani P (2021) Decomposing the performance metrics of coconut cultivation in the South Indian States. Humanit Soc Sci Commun 8(1):114. https://doi.org/10.1057/s41599-021-00783-0
40. Becker WM, Petersen A, Jappe U (2018) Peanut allergens: new consolidated findings on structure. Char Allergom Allergol Sel 2(01):67–79. https://doi.org/10.5414/ALX01418E
41. Magnabosco G, Giuri D, Di Bisceglie AP, Scarpino F, Fermani S, Tomasini C, Falini G (2021) New material perspective for waste seashells by covalent functionalization. ACS Sustain Chem Eng 9(18):6203–6208. https://doi.org/10.1021/acssuschemeng.1c01306
42. Mo KH, Alengaram UJ, Jumaat MZ, Lee SC, Goh WI, Yuen CW (2018) Recycling of seashell waste in concrete: a review. Constr Build Mater 162:751–764. https://doi.org/10.1016/j.conbuildmat.2017.12.009
43. Hincke, Maxwell T (2012) The eggshell: structure, composition and mineralization. Front Biosci 17(1):1266. https://doi.org/10.2741/3985
44. Witoon T (2011) Characterization of calcium oxide derived from waste eggshell and its application as CO2 sorbent. Ceram Int 37(8):3291–3298. https://doi.org/10.1016/J.CERAMINT.2011.05.125
45. Nath D, Jangid K, Susaniya A, Kumar R, Vaish R (2021) Eggshell derived CaO-portland cement antibacterial composites. Compos Part C Open Access 5:100123. https://doi.org/10.1016/j.jcomc.2021.100123
46. Cree D, Pliya P (2019) Effect of elevated temperature on eggshell, eggshell powder and eggshell powder mortars for masonry applications. J Build Eng 26:100852. https://doi.org/10.1016/j.jobe.2019.100852
47. Jaiswal KK, Dutta S, Pohrmen CB, Verma R, Kumar A, Ramaswamy AP (2021) Bio-waste chicken eggshell-derived calcium oxide for photocatalytic application in methylene blue dye degradation under natural sunlight irradiation. Inorg Nano-Metal Chem 51(7):995–1004. https://doi.org/10.1080/24701556.2020.1813769
48. Ahmad W, Sethupathi S, Munusamy Y, Kanthasamy R (2021) Valorization of raw and calcined chicken eggshell for sulfur dioxide and hydrogen sulfide removal at low temperature. Catalysts 11(2):295. https://doi.org/10.3390/catal11020295
49. Jalu RG, Chamada TA, Kasirajan DR (2021) Calcium oxide nanoparticles synthesis from hen eggshells for removal of lead (Pb(II)) from aqueous solution. Environ Challenges 4:100193. https://doi.org/10.1016/j.envc.2021.100193
50. Fayyazi E, Ghobadian B, van de Bovenkamp HH, Najafi G, Hosseinzadehsamani B, Heeres HJ, Yue J (2018) Optimization of biodiesel production over chicken eggshell-derived CaO catalyst in a continuous centrifugal contactor separator. Ind Eng Chem Res 57(38):12742–12755. https://doi.org/10.1021/acs.iecr.8b02678
51. Zhang M, Ramya G, Brindhadevi K, Alsehli M, Elfasakhany A, Xia C, Lan Chi NT, Pugazhendhi A (2022) Microwave assisted biodiesel production from chicken feather meal oil

using bio-nano calcium oxide derived from chicken egg shell. Environ Res 205:112509. https://doi.org/10.1016/j.envres.2021.112509
52. Habte L, Shiferaw N, Mulatu D, Thenepalli T, Chilakala R, Ahn J (2019) Synthesis of nano-calcium oxide from waste eggshell by sol-gel method. Sustainability 11(11):3196. https://doi.org/10.3390/su11113196
53. Hsieh S-L, Li F-Y, Lin P-Y, Beck DE, Kirankumar R, Wang G-J, Hsieh S (2021) CaO recovered from eggshell waste as a potential adsorbent for greenhouse gas CO2. J Environ Manage 297:113430. https://doi.org/10.1016/j.jenvman.2021.113430
54. Kaewdaeng S, Sintuya P, Nirunsin R (2017) Biodiesel production using calcium oxide from river snail shell ash as catalyst. Energy Procedia 138:937–942. https://doi.org/10.1016/j.egypro.2017.10.057
55. Agwu OE, Akpabio JU, Akpabio MG (2020) Potentials of waste seashells as additives in drilling muds and in oil well cements. Clean Eng Technol 1:100008. https://doi.org/10.1016/j.clet.2020.100008
56. Chilakala R, Thannaree C, Shin EJ, Thenepalli T, Ahn JW (2019) Sustainable solutions for oyster shell waste recycling in Thailand and the Philippines. Recycling 4(3):35. https://doi.org/10.3390/recycling4030035
57. Marques Correia L, Cecilia JA, Rodríguez-Castellón E, Cavalcante CL, Vieira RS (2017) Relevance of the physicochemical properties of calcined quail eggshell (CaO) as a catalyst for biodiesel production. J Chem 2017:1–12. https://doi.org/10.1155/2017/5679512
58. Vivek S, Sophia M (2019) Efficient management of egg shell and conch shell wastes by utilization as bio fillers in eco friendly gypsum mortar. Int J Eng Adv Technol 9(2):5590–5596. https://doi.org/10.35940/ijeat.B2509.129219
59. Leelatawonchai P, Laonapakul T (2014) Preparation and characterization of calcium sources from golden apple snail shell for naturally based biomaterials. Adv Mater Res 931–932:370–374. https://doi.org/10.4028/www.scientific.net/AMR.931-932.370
60. Laskar IB, Rajkumari K, Gupta R, Chatterjee S, Paul B, Rokhum SL (2018) Waste snail shell derived heterogeneous catalyst for biodiesel production by the transesterification of soybean oil. RSC Adv 8(36):20131–20142. https://doi.org/10.1039/C8RA02397B
61. Buasri A, Chaiyut N, Loryuenyong V, Worawanitchaphong P, Trongyong S (2013) Calcium oxide derived from waste shells of mussel, cockle, and scallop as the heterogeneous catalyst for biodiesel production. Sci World J 2013:1–7. https://doi.org/10.1155/2013/460923
62. Venkat Reddy CR, Oshel R, Verkade JG (2006) Room-temperature conversion of soybean oil and poultry fat to biodiesel catalyzed by nanocrystalline calcium oxides. Energy Fuels 20(3):1310–1314. https://doi.org/10.1021/ef050435d
63. Hindarso H, Epriliati I, Hoerudin D, Yuliani S (2021) Synthesis and characterization of biosilica from rice husks as a catalyst for the production of biodiesel. Fine Chem Eng 2:39–44. https://doi.org/10.37256/fce.222021735
64. Park JY, Mun W, Chun J, Sang B-I, Mitchell RJ, Lee JH (2022) Alkali extraction to detoxify rice husk-derived silica and increase its biocompatibility. ACS Sustain Chem Eng 10(24):7811–7817. https://doi.org/10.1021/acssuschemeng.2c01307
65. Petrache Voicu S, Dinu D, Sima C, Hermenean A, Ardelean A, Codrici E, Stan M, Zărnescu O, Dinischiotu A (2015) Silica Nanoparticles induce oxidative stress and autophagy but not apoptosis in the MRC-5 cell line. Int J Mol Sci 16(12):29398–29416. https://doi.org/10.3390/ijms161226171
66. Haq IU, Akhtar K, Malik A (2014) Effect of experimental variables on the extraction of silica from the rice husk ash. J Chem Soc Pakistan 36(3):382–387
67. Dorairaj D, Govender N, Zakaria S, Wickneswari R (2022) Green synthesis and characterization of UKMRC-8 rice husk-derived mesoporous silica nanoparticle for agricultural application. Sci Rep 12(1):20162. https://doi.org/10.1038/s41598-022-24484-z
68. Le VH, Thuc CNH, Thuc HH (2013) Synthesis of silica nanoparticles from Vietnamese rice husk by sol-gel method. Nanoscale Res Lett 8(1):58. https://doi.org/10.1186/1556-276X-8-58
69. Real C, Alcala MD, Criado JM (1996) Preparation of silica from rice husks. J Am Ceram Soc 79(8):2012–2016. https://doi.org/10.1111/j.1151-2916.1996.tb08931.x
70. Kalapathy U (2000) A simple method for production of pure silica from rice hull ash. Bioresour Technol 73(3):257–262. https://doi.org/10.1016/S0960-8524(99)00127-3
71. Kalapathy U, Proctor A, Shultz J (2002) An improved method for production of silica from rice hull ash. Bioresour Technol 85(3):285–289. https://doi.org/10.1016/S0960-8524(02)00116-5
72. Liou T-H, Yang C-C (2011) Synthesis and surface characteristics of nanosilica produced from alkali-extracted rice husk ash. Mater Sci Eng B 176(7):521–529. https://doi.org/10.1016/j.mseb.2011.01.007
73. Schlomach J, Kind M (2004) Investigations on the semi-batch precipitation of silica. J Colloid Interface Sci 277(2):316–326. https://doi.org/10.1016/j.jcis.2004.04.051
74. Pa FC, Kein WK (2019) Removal of iron in rice husk via oxalic acid leaching process. IOP Conf Ser Mater Sci Eng 701(1):012021. https://doi.org/10.1088/1757-899X/701/1/012021
75. Mehdinia SM, Latif PA, Abdullah AM, Taghipour H (2011) Synthesize and characterization of rice husk silica to remove the hydrogen sulfide through the physical filtration system. Asian J Sci Res 4(3):246–254. https://doi.org/10.3923/ajsr.2011.246.254
76. Bakar RA, Yahya R, Gan SN (2016) Production of high purity amorphous silica from rice husk. Procedia Chem 19:189–195. https://doi.org/10.1016/j.proche.2016.03.092
77. Guo W, Li G, Zheng Y, Li K (2021) Nano-silica extracted from rice husk and its application in acetic acid steam reforming. RSC Adv 11(55):34915–34922. https://doi.org/10.1039/D1RA05255A
78. September LA, Kheswa N, Seroka NS, Khotseng L (2023) Green synthesis of silica and silicon from agricultural residue sugarcane bagasse ash – a mini review. RSC Adv 13(2):1370–1380. https://doi.org/10.1039/D2RA07490G
79. Bahurudeen A, Santhanam M (2015) Influence of different processing methods on the pozzolanic performance of sugarcane bagasse ash. Cem Concr Compos 56:32–45. https://doi.org/10.1016/j.cemconcomp.2014.11.002
80. Norsuraya S, Fazlena H, Norhasyimi R (2016) Sugarcane bagasse as a renewable source of silica to synthesize Santa Barbara amorphous-15 (SBA-15). Procedia Eng 148:839–846. https://doi.org/10.1016/j.proeng.2016.06.627
81. Bortolotto Teixeira L, Guzi de Moraes E, Paolinelli Shinhe G, Falk G, Novaes de Oliveira AP (2021) Obtaining biogenic silica from sugarcane bagasse and leaf ash. Waste Biomass Valor 12(6):3205–3221. https://doi.org/10.1007/s12649-020-01230-y
82. Rovani S, Santos JJ, Corio P, Fungaro DA (2018) Highly pure silica nanoparticles with high adsorption capacity obtained from sugarcane waste ash. ACS Omega 3(3):2618–2627. https://doi.org/10.1021/acsomega.8b00092
83. Vaibhav V, Vijayalakshmi U, Roopan SM (2015) Agricultural waste as a source for the production of silica nanoparticles. Spectrochim Acta Part A Mol Biomol Spectrosc 139:515–520. https://doi.org/10.1016/j.saa.2014.12.083
84. Chindaprasirt P, Rattanasak U (2020) Eco-production of silica from sugarcane bagasse ash for use as a photochromic pigment filler. Sci Rep 10(1):9890. https://doi.org/10.1038/s41598-020-66885-y

85. Anuar MF, Fen YW, Zaid MHM, Matori KA, Khaidir REM (2018) Synthesis and structural properties of coconut husk as potential silica source. Results Phys 11:1–4. https://doi.org/10.1016/j.rinp.2018.08.018
86. Norul Azlin MZ, Syamim Syufiana S (2022) The Preparation and Characterization of Silica from Coconut Husk. J Phys Conf Ser 2266(1):012011. https://doi.org/10.1088/1742-6596/2266/1/012011
87. Saghiri MA, Orangi J, Asatourian A, Gutmann JL, Garcia-Godoy F, Lotfi M, Sheibani N (2017) Calcium silicate-based cements and functional impacts of various constituents. Dent Mater J 36(1):8. https://doi.org/10.4012/DMJ.2015-425
88. Ernawati L, Yusariarta AW, Alviany R, Halim A (2022) Effect of CaO/SiO 2 compositions on the structure formation of mesoporous calcium silicate (CaSiO 3) composite particles as adsorbent for organic dye removal. IOP Conf Ser Earth Environ Sci 963(1):012008. https://doi.org/10.1088/1755-1315/963/1/012008
89. Hossain SS, Roy PK (2018) Study of physical and dielectric properties of bio-waste-derived synthetic wollastonite. J Asian Ceram Soc 6(3):289–298. https://doi.org/10.1080/21870764.2018.1508549
90. Mazzucato E, Gualtieri AF (2000) Wollastonite polytypes in the CaO-SiO 2 system. Phys Chem Miner 27(8):565–574. https://doi.org/10.1007/s002690000095
91. Seryotkin YV, Sokol EV, Kokh SN (2012) Natural pseudowollastonite: crystal structure, associated minerals, and geological context. Lithos 134–135:75–90. https://doi.org/10.1016/j.lithos.2011.12.010
92. Azarov GM, Maiorova EV, Oborina MA, Belyakov AV (1995) Wollastonite raw materials and their applications (a review). Glas Ceram 52(9):237–240. https://doi.org/10.1007/BF00681090
93. Przywecka K, Kowalczyk K, Grzmil B (2020) Sequential Co-precipitation as a convenient preparation method of anticorrosive hybrid calcium phosphate/calcium silicate powder pigments. Powder Technol 373:660–670. https://doi.org/10.1016/j.powtec.2020.07.003
94. Leite FHG, Almeida TF, Faria RT, Holanda JNF (2017) Synthesis and characterization of calcium silicate insulating material using avian eggshell waste. Ceram Int 43(5):4674–4679. https://doi.org/10.1016/j.ceramint.2016.12.146
95. Dhoble SJ, Dhoble NS, Pode RB (2003) Preparation and characterization of Eu3+ activated CaSiO3, (CaA)SiO3 [A = Ba or Sr] phosphors. Bull Mater Sci 26(4):377–382. https://doi.org/10.1007/BF02711179
96. Khristov TI, Popovich NV, Galaktionov SS, Soshchin NP (1994) Calcium silicate phosphors obtained by the sol-gel method. Glas Ceram 51(9–10):290–296. https://doi.org/10.1007/BF00679827
97. Wang S, Peng X, Tang L, Cao C, Zeng L (2018) Contact-hardening behavior of calcium silicate hydrate powders. Materials (Basel) 11(12):2367. https://doi.org/10.3390/ma11122367
98. Navas D, Fuentes S, Castro-Alvarez A, Chavez-Angel E (2021) Review on sol-gel synthesis of perovskite and oxide nanomaterials. Gels 7(4):275. https://doi.org/10.3390/gels7040275
99. Bokov D, Turki Jalil A, Chupradit S, Suksatan W, Javed Ansari M, Shewael IH, Valiev GH, Kianfar E (2021) Nanomaterial by sol-gel method: synthesis and application. Adv Mater Sci Eng 2021. https://doi.org/10.1155/2021/5102014
100. Harish V, Ansari MM, Tewari D, Gaur M, Yadav AB, García-Betancourt M-L, Abdel-Haleem FM, Bechelany M, Barhoum A (2022) Nanoparticle and nanostructure synthesis and controlled growth methods. Nanomaterials 12(18):3226. https://doi.org/10.3390/nano12183226
101. Liu C, Shaw L (2016) Nanoparticulate materials and core/shell structures derived from wet chemistry methods. In: Encyclopedia of nanotechnology; Springer Netherlands: Dordrecht , pp 2579–2597. https://doi.org/10.1007/978-94-017-9780-1_100906
102. Jagadale PN, Kulal SR, Joshi MG, Jagtap PP, Khetre SM, Bamane SR (2013) Synthesis and characterization of nanostructured casio3 biomaterial. Mater Sci 31(2):269–275. https://doi.org/10.2478/s13536-012-0099-8
103. Xue W, Bandyopadhyay A, Bose S (2009) Mesoporous calcium silicate for controlled release of bovine serum albumin protein. Acta Biomater 5(5):1686–1696. https://doi.org/10.1016/j.actbio.2009.01.012
104. Lin K, Chang J, Chen G, Ruan M, Ning C (2007) A simple method to synthesize single-crystalline β-wollastonite nanowires. J Cryst Growth 300(2):267–271. https://doi.org/10.1016/j.jcrysgro.2006.11.215
105. Pei LZ, Yang LJ, Yang Y, Fan CG, Yin WY, Chen J, Zhang QF (2010) A green and facile route to synthesize calcium silicate nanowires. Mater Charact 61(11):1281–1285. https://doi.org/10.1016/j.matchar.2010.07.002
106. Li X, Chang J (2004) Synthesis of wollastonite single crystal nanowires by a novel hydrothermal route. Chem Lett 33(11):1458–1459. https://doi.org/10.1246/cl.2004.1458
107. Lin K, Chang J, Lu J (2006) Synthesis of wollastonite nanowires via hydrothermal microemulsion methods. Mater Lett 60(24):3007–3010. https://doi.org/10.1016/j.matlet.2006.02.034
108. Phuttawong R, Chantaramee N, Pookmanee P, Puntharod R (2015) Synthesis and characterization of calcium silicate from rice husk ash and shell of snail *Pomacea Canaliculata* by solid state reaction. Adv Mater Res 1103:1–7. https://doi.org/10.4028/WWW.SCIENTIFIC.NET/AMR.1103.1
109. Kaur Chhina M, Singh K (2021) Samarium doped calcium silicate derived from agro-food wastes and their structural optical luminescent properties. Ceram Int 47(15):21588–21598. https://doi.org/10.1016/J.CERAMINT.2021.04.171
110. Palakurthy S, Azeem PA, Venugopal Reddy K, Penugurti V, Manavathi B (2020) A comparative study on in vitro behavior of calcium silicate ceramics synthesized from biowaste resources. J Am Ceram Soc 103(2):933–943. https://doi.org/10.1111/jace.16745
111. Kaou MH, Horváth ZE, Balázsi K, Balázsi C (2023) Eco-friendly preparation and structural characterization of calcium silicates derived from eggshell and silica gel. Int J Appl Ceram Technol 20(2):689–699. https://doi.org/10.1111/ijac.14274
112. Yudha SS, Falahudin A, Kaus NHM, Thongmee S, Ikram S, Asdim A (2020) Preliminary synthesis of calcium silicates using oil palm leaves and eggshells. Bull Chem React Eng Catal 15(2):561–567. https://doi.org/10.9767/bcrec.15.2.7591.561-567
113. Sharma G, Singh K (2022) Dielectric properties of the calcium silicate glass-ceramics prepared from agro-food wastes. Silicon 14(4):1489–1496. https://doi.org/10.1007/s12633-021-00940-9
114. Reddappa R, Devi LL, Babu P, Martín IR, Lavín V, Venkatramu V, Rodríguez-Mendoza UR, Jayasankar CK (2022) Structural, morphological and photoluminescence properties of Ca2SiO4:Er3+ phosphors synthesized from agro-food waste materials. Ceram Int 48(24):37013–37019. https://doi.org/10.1016/j.ceramint.2022.08.271
115. Reddappa R, Devi LL, Basavapoornima C, Depuru SR, Kaewkhao J, Pecharapa W, Jayasankar CK (2022) Photoluminescence characteristics of Ln3+-doped phosphors derived from sustainable resources for solid state lightning applications. Optik (Stuttg) 264(March):169360. https://doi.org/10.1016/j.ijleo.2022.169360
116. Nayak JP, Kumar S, Bera J (2010) Sol-gel synthesis of bioglass-ceramics using rice husk ash as a source for silica and its characterization. J Non Cryst Solids 356(28–30):1447–1451. https://doi.org/10.1016/j.jnoncrysol.2010.04.041

117. Ismail H, Shamsudin R, Hamid MAA, Jalar A (2013) Synthesis and characterization of nano-wollastonite from rice husk ash and limestone. Mater Sci Forum 756:43–47. https://doi.org/10.4028/www.scientific.net/MSF.756.43
118. Choudhary R, Koppala S, Swamiappan S (2015) Bioactivity studies of calcium magnesium silicate prepared from eggshell waste by sol-gel combustion synthesis. J Asian Ceram Soc 3(2):173–177. https://doi.org/10.1016/j.jascer.2015.01.002
119. Mohammadi H, Hei BZ, Ismail YMB, Shariff KA, Noor AFM (2020) Green synthesis of calcium magnesium silicate (cms-akermanite) using natural biowastes by solid-state sintering route. Malaysian J Microsc 16(2):66–76
120. Punj S, Singh K (2020) Bioactive calcium silicate glass synthesized from sustainable biomass wastes. Biofuels Bioprod Biorefin 14(6):1141–1151. https://doi.org/10.1002/bbb.2135
121. Venkatraman SK, Choudhary R, Krishnamurithy G, Balaji Raghavendran HR, Murali MR, Kamarul T, Suresh A, Abraham J, Praharaj S, Swamiappan S (2022) Comparative investigation on antibacterial, biological and mechanical behaviour of monticellite and diopside derived from biowaste for bone regeneration. Mater Chem Phys 286:126157. https://doi.org/10.1016/j.matchemphys.2022.126157
122. Vijayakumar N, Venkatraman SK, Choudhary R, Indurkar A, Chatterjee A, Abraham J, Ostrovskiy S, Senatov F, Locs J, Swamiappan S (2022) Conversion of biowaste into larnite by sol-gel combustion route for biomedical applications. Chemistry Select 7(4). https://doi.org/10.1002/slct.202103783
123. Kunjalukkal Padmanabhan S, Nitti P, Stanca E, Rochira A, Siculella L, Raucci MG, Madaghiele M, Licciulli A, Demitri C (2021) Mechanical and biological properties of magnesium- and silicon-substituted hydroxyapatite scaffolds. Materials (Basel) 14(22):6942. https://doi.org/10.3390/ma14226942
124. Gao C, Peng S, Feng P, Shuai C (2017) Bone biomaterials and interactions with stem cells. Bone Res 5(1):17059. https://doi.org/10.1038/boneres.2017.59
125. Maeno S, Niki Y, Matsumoto H, Morioka H, Yatabe T, Funayama A, Toyama Y, Taguchi T, Tanaka J (2005) The effect of calcium ion concentration on osteoblast viability, proliferation and differentiation in monolayer and 3D culture. Biomaterials 26(23):4847–4855. https://doi.org/10.1016/j.biomaterials.2005.01.006
126. Zhou R, Guo Q, Xiao Y, Guo Q, Huang Y, Li C, Luo X (2021) Endocrine role of bone in the regulation of energy metabolism. Bone Res 9(1):25. https://doi.org/10.1038/s41413-021-00142-4
127. Zhang Q, Riddle RC, Clemens TL (2015) Bone and the regulation of global energy balance. J Intern Med 277(6):681–689. https://doi.org/10.1111/joim.12348
128. Price CT, Koval KJ, Langford JR (2013) Silicon: a review of its potential role in the prevention and treatment of postmenopausal osteoporosis. Int J Endocrinol 2013:1–6. https://doi.org/10.1155/2013/316783
129. Nasser Atia GA, Barai HR, Shalaby HK, Ali NG, Morsy SM, Ghobashy M, Mohamady, Nasser Attia HA, Joo SW (2022) Baghdadite: a novel and promising calcium silicate in regenerative dentistry and medicine. ACS Omega 7(49):44532–44541. https://doi.org/10.1021/acsomega.2c05596
130. Shie M-Y, Ding S-J, Chang H-C (2011) The role of silicon in osteoblast-like cell proliferation and apoptosis. Acta Biomater 7(6):2604–2614. https://doi.org/10.1016/j.actbio.2011.02.023
131. Huang Y, Jin X, Zhang X, Sun H, Tu J, Tang T, Chang J, Dai K (2009) In vitro and in vivo evaluation of akermanite bioceramics for bone regeneration. Biomaterials 30(28):5041–5048. https://doi.org/10.1016/j.biomaterials.2009.05.077
132. Moghadasi K, Mohd Isa MS, Ariffin MA, Mohd Jamil MZ, Raja S, Wu B, Yamani M, Bin Muhamad MR, Yusof F, Jamaludin MF, Ab Karim MS bin, Abdul Razak B binti, Yusoff N bin (2022) A review on biomedical implant materials and the effect of friction stir based techniques on their mechanical and tribological properties. J Mater Res Technol 17:1054–1121. https://doi.org/10.1016/j.jmrt.2022.01.050
133. Yamamoto A, Honma R, Sumita M, Hanawa T (2004) Cytotoxicity evaluation of ceramic particles of different sizes and shapes. J Biomed Mater Res 68A(2):244–256. https://doi.org/10.1002/jbm.a.20020
134. Chen J, Tan L, Yu X, Etim IP, Ibrahim M, Yang K (2018) Mechanical properties of magnesium alloys for medical application: a review. J Mech Behav Biomed Mater 87:68–79. https://doi.org/10.1016/j.jmbbm.2018.07.022
135. Zhang T, Wang W, Liu J, Wang L, Tang Y, Wang KA (2022) Review on magnesium alloys for biomedical applications. Front Bioeng Biotechnol 10:953344. https://doi.org/10.3389/fbioe.2022.953344
136. Saud AN, Koç E, Özdemir O (2023) Characterization and in vitro bioactivity analysis of apatite growth on modified calcium borate silicate ceramic. Ceram Int. https://doi.org/10.1016/j.ceramint.2023.06.002
137. Weng J (1997) Formation and characteristics of the apatite layer on plasma-sprayed hydroxyapatite coatings in simulated body fluid. Biomaterials 18(15):1027–1035. https://doi.org/10.1016/S0142-9612(97)00022-7
138. Sun J, Li J, Liu X, Wei L, Wang G, Meng F (2009) Proliferation and gene expression of osteoblasts cultured in DMEM containing the ionic products of dicalcium silicate coating. Biomed Pharmacother 63(9):650–657. https://doi.org/10.1016/j.biopha.2009.01.007
139. Sun M, Liu A, Ma C, Shao H, Yu M, Liu Y, Yan S, Gou Z (2016) Systematic investigation of β-dicalcium silicate-based bone cements in vitro and in vivo in comparison with clinically applied calcium phosphate cement and bio-Oss®. RSC Adv 6(1):586–596. https://doi.org/10.1039/C5RA21340A
140. Siriphannon P, Kameshima Y, Yasumori A, Okada K, Hayashi S (2002) Formation of hydroxyapatite on CaSiO3 powders in simulated body fluid. J Eur Ceram Soc 22(4):511–520. https://doi.org/10.1016/S0955-2219(01)00301-6
141. Xue W, Liu X, Zheng X, Ding C (2005) In vivo evaluation of plasma-sprayed wollastonite coating. Biomaterials 26(17):3455–3460. https://doi.org/10.1016/j.biomaterials.2004.09.027
142. Xu S, Lin K, Wang Z, Chang J, Wang L, Lu J, Ning C (2008) Reconstruction of calvarial defect of rabbits using porous calcium silicate bioactive ceramics. Biomaterials 29(17):2588–2596. https://doi.org/10.1016/j.biomaterials.2008.03.013
143. Du Z, Leng H, Guo L, Huang Y, Zheng T, Zhao Z, Liu X, Zhang X, Cai Q, Yang X (2020) calcium silicate scaffolds promoting bone regeneration via the doping of Mg2+ or Mn2+ Ion. Compos Part B Eng 190:107937. https://doi.org/10.1016/j.compositesb.2020.107937
144. Shao H, Ke X, Liu A, Sun M, He Y, Yang X, Fu J, Liu Y, Zhang L, Yang G, Xu S, Gou Z (2017) Bone regeneration in 3d printing bioactive ceramic scaffolds with improved tissue/material interface pore architecture in thin-wall bone defect. Biofabrication 9(2):025003. https://doi.org/10.1088/1758-5090/aa663c
145. Wu C, Chang J (2006) A novel akermanite bioceramic: preparation and characteristics. J Biomater Appl 21(2):119–129. https://doi.org/10.1177/0885328206057953
146. Xia L, Yin Z, Mao L, Wang X, Liu J, Jiang X, Zhang Z, Lin K, Chang J, Fang B (2016) Akermanite bioceramics promote osteogenesis, angiogenesis and suppress osteoclastogenesis for osteoporotic bone regeneration. Sci Rep 6(February):1–17. https://doi.org/10.1038/srep22005
147. Nonami T (1991) Developmental study of diopside for use as implant material. MRS Proc 252:87. https://doi.org/10.1557/PROC-252-87

148. Vichaphund S, Kitiwan M, Atong D, Thavorniti P (2011) Microwave synthesis of wollastonite powder from eggshells. J Eur Ceram Soc 31(14):2435–2440. https://doi.org/10.1016/j.jeurceramsoc.2011.02.026
149. Anjaneyulu U, Sasikumar S (2014) Bioactive nanocrystalline wollastonite synthesized by sol-gel combustion method by using eggshell waste as calcium source. Bull Mater Sci 37(2):207–212. https://doi.org/10.1007/s12034-014-0646-5
150. Abd Rashid R, Shamsudin R, Abdul Hamid MA, Jalar A (2014) In-vitro bioactivity of wollastonite materials derived from limestone and silica sand. Ceram Int 40(5):6847–6853. https://doi.org/10.1016/j.ceramint.2013.12.004
151. Saravanan S, Vimalraj S, Vairamani M, Selvamurugan N (2015) Role of mesoporous wollastonite (calcium silicate) in mesenchymal stem cell proliferation and osteoblast differentiation: a cellular and molecular study. J Biomed Nanotechnol 11(7):1124–1138. https://doi.org/10.1166/jbn.2015.2057
152. De Jong WH, Borm PJA (2008) Drug delivery and nanoparticles: applications and hazards. Int J Nanomed 3(2):133–149. https://doi.org/10.2147/IJN.S596
153. Li C, Wang J, Wang Y, Gao H, Wei G, Huang Y, Yu H, Gan Y, Wang Y, Mei L, Chen H, Hu H, Zhang Z, Jin Y (2019) Recent progress in drug delivery. Acta Pharm Sin B 9(6):1145–1162. https://doi.org/10.1016/j.apsb.2019.08.003
154. Zhu Y-J (2017) Nanostructured materials of calcium phosphates and calcium silicates: synthesis properties and applications Chinese. J Chem 35(6):769–790. https://doi.org/10.1002/cjoc.201600696
155. Elmore AR, Cosmetic Ingredient Review Expert Panel (2003) Final report on the safety assessment of aluminum silicate, calcium silicate, magnesium aluminum silicate, magnesium silicate, magnesium trisilicate, sodium magnesium silicate, zirconium silicate, attapulgite, bentonite, Fuller's earth, hectorite, kaolin, lithium magnesium silicate, lithium magnesium sodium silicate, montmorillonite, pyrophyllite, and zeolite. Int J Toxicol 22:37–102. https://doi.org/10.1177/1091581803022S115156
156. Wu J, Zhu Y-J, Cao S-W, Chen F (2010) Hierachically nanostructured mesoporous spheres of calcium silicate hydrate: surfactant-free sonochemical synthesis and drug-delivery system with ultrahigh drug-loading capacity. Adv Mater 22(6):749–753. https://doi.org/10.1002/adma.200903020
157. Zhang M, Chang J (2010) Surfactant-assisted sonochemical synthesis of hollow calcium silicate hydrate (CSH) microspheres for drug delivery. Ultrason Sonochem 17(5):789–792. https://doi.org/10.1016/j.ultsonch.2010.01.012
158. Fan Y, Huang S, Jiang J, Li G, Yang P, Lian H, Cheng Z, Lin J (2011) Luminescent, mesoporous, and bioactive europium-doped calcium silicate (MCS: Eu3+) as a drug carrier. J Colloid Interface Sci 357(2):280–285. https://doi.org/10.1016/j.jcis.2011.01.109
159. Kang X, Huang S, Yang P, Ma P, Yang D, Lin J (2011) Preparation of luminescent and mesoporous Eu 3+ /Tb 3+ doped calcium silicate microspheres as drug carriers via a template route. Dalt Trans 40(9):1873–1879. https://doi.org/10.1039/C0DT01390K
160. Verma S, Kumar D, Dutta S, Sharma V, Swart HC, Kumar V (2020) A Novel near white light emitting phosphor KSrYSi2O7:Dy3+: synthesis. Characterization and Luminescence Properties Vacuum 174:109179. https://doi.org/10.1016/j.vacuum.2020.109179
161. Al-Shetwi AQ (2022) Sustainable development of renewable energy integrated power sector: trends, environmental impacts, and recent challenges. Sci Total Environ 822:153645. https://doi.org/10.1016/j.scitotenv.2022.153645
162. Tiwari G, Brahme N, Sharma R, Bisen DP, Sao SK, Tigga S (2016) Luminescence properties of dysprosium doped di-calcium di-aluminium silicate phosphors. Opt Mater (Amst) 58:234–242. https://doi.org/10.1016/j.optmat.2016.05.033
163. Krishnan R, Shibu SN, Poelman D, Badyal AK, Kunti AK, Swart HC, Menon SG (2022) Recent advances in microwave synthesis for photoluminescence and photocatalysis. Mater Today Commun 32:03890, 1. https://doi.org/10.1016/j.mtcomm.2022.103890
164. Barve RA, Suriyamurthy N, Panigrahi BS, Venkatraman B (2015) Optical properties and judd-ofelt analysis of Eu3+ activated calcium silicate. Phys B Condens Matter 475:156–161. https://doi.org/10.1016/j.physb.2015.07.029
165. Woo H-J, Gandhi S, Kwon B-J, Shin D-S, Yi SS, Jeong JH, Jang K (2015) Soluble silica assisted synthesis and luminescent characteristics of yellow emitting CaSrSiO4:Eu2+ phosphors for warm white light production. Ceram Int 41(4):5547–5553. https://doi.org/10.1016/j.ceramint.2014.12.131
166. Kojima Y, Kamei S, Nishimiya N (2010) Preparation and fluorescence property of red-emitting Eu3+-activated amorphous calcium silicate phosphor. Mater Res Bull 45(2):121–123. https://doi.org/10.1016/j.materresbull.2009.09.032
167. Upendra Rao MS, Hanumantharayappa C, Ramesh KP, Haranath D (2019) Effect of alkali charge compensator on luminescent properties in Eu3+ doped β-dicalcium silicate. Optik (Stuttg) 178:1255–1263. https://doi.org/10.1016/j.ijleo.2018.10.015
168. Tseng HW, Tu HY, Yang QH, Yang CF (2022) Effects of composition variations on the crystalline phases and photoluminescence properties of Ca2+ XMgSi2Eu0.025O7+ XPhosphors. ACS Omega 7(5):3917–3924. https://doi.org/10.1021/acsomega.1c04480
169. Fei Q, Chang C, Mao D (2005) Luminescent properties of Sr2MgSi2O7 and Ca2MgSi2O7 long lasting phosphors activated by Eu2+, Dy3+. J Alloys Compd 390(1–2):133–137. https://doi.org/10.1016/J.JALLCOM.2004.06.096
170. Cao H, Liu M, Chen H (2019) The luminescent properties of long afterglow phosphors: Ca2MgSi2O7: Eu2+, Tm3+ with different preparation temperatures. Phys B Condens Matter 571:243–246. https://doi.org/10.1016/j.physb.2019.07.013
171. Dewangan P, Bisen DP, Brahme N, Sharma S (2019) Structural characterization and luminescence properties of Dy3+ doped Ca3MgSi2O8 phosphors. J Alloys Compd 777:423–433. https://doi.org/10.1016/j.jallcom.2018.10.390
172. Husain S, Haryanti NH, Suryajaya S, Permitaria A (2019) Synthesis and characterization of calcium silicate from rice husk ash and snail shell. J Neutrino 11(2):45. https://doi.org/10.18860/neu.v11i2.6608
173. Palakurthy S, Venu Gopal Reddy K, Samudrala RK, Abdul Azeem P (2019) In vitro bioactivity and degradation behaviour of β-wollastonite derived from natural waste. Mater Sci Eng C 98:109–117. https://doi.org/10.1016/J.MSEC.2018.12.101
174. Yadav P, Raju MK, Samudrala RK, Gangadhar M, Pani J, Borkar H, Azeem PA (2023) Cost-effective akermanite derived from industrial waste for working electrodes in supercapacitor applications. New J Chem 47(7):3255–3265. https://doi.org/10.1039/D2NJ05066H
175. Krishnam Raju M, Prasada Rao R, Vijayan N, Abdul Azeem P (2021) A Novel orange-red Sm3+-doped CaSiO3 nanostructured phosphor derived from agro food waste materials for white light applications. Ceram Int 47(19):26704–26711. https://doi.org/10.1016/J.CERAMINT.2021.06.077
176. Priya R, Khurana I, Pandey OP (2020) Synthesis of intense red light-emitting β-Ca2SiO4:Eu3+ phosphors for near UV-excited light-emitting diodes utilizing agro-food waste materials. J Mater

Sci Mater Electron 31(3):1912–1928. https://doi.org/10.1007/S10854-019-02710-1
177. Srinath P, Abdul Azeem P, Venugopal Reddy K, Chiranjeevi P, Bramanandam M, Prasada Rao R (2021) A novel cost-effective approach to fabricate diopside bioceramics: a promising ceramics for orthopedic applications. Adv Powder Technol 32(3):875–884. https://doi.org/10.1016/j.apt.2021.01.038
178. Danewalia SS, Sharma G, Thakur S, Singh K (2016) agricultural wastes as a resource of raw materials for developing low-dielectric glass-ceramics. Sci Rep 6(1):24617. https://doi.org/10.1038/srep24617
179. Jakfar NH, Fhan KS, Johar B, Shima Adzali NM, Mohd Yunus SNH, Meng CE (2021) Crystal structure and thermal behaviour of calcium monosilicate derived from calcined chicken eggshell and rice husk ash. J Phys Conf Ser 2129 (1):012040. https://doi.org/10.1088/1742-6596/2129/1/012040
180. Minakshi M, Higley S, Baur C, Mitchell DRG, Jones RT, Fichtner M (2019) Calcined chicken eggshell electrode for battery and supercapacitor applications. RSC Adv 9(46):26981–26995. https://doi.org/10.1039/C9RA04289J
181. Patel KG, Shettigar RR, Misra NM (2017) Recent advance in silica production technologies from agricultural waste stream–review. J Adv Agric Technol 4(3):274–279. https://doi.org/10.18178/joaat.4.3.274-279
182. Anuar MF, Fen YW, Zaid MHM, Matori KA, Khaidir REM (2020) The physical and optical studies of crystalline silica derived from the green synthesis of coconut husk ash. Appl Sci 10(6):2128. https://doi.org/10.3390/app10062128